Microemulsion Liquid Crystal Templates for Highly Ordered Three-Dimensional Mesoporous Silica Monoliths with Controllable Mesopore Structures

S. A. El-Safty* and T. Hanaoka†

Laboratory for Membrane Chemistry, Tohoku Center, National Institute of Advanced Industrial Science and Technology (AIST), 4-2-1 Nigatake, Miyagino-ku, Sendai, 983-8551, Japan

Received April 20, 2003. Revised Manuscript Received November 6, 2003

Nanostructure composite silica monoliths (HOM-*n*) with three-dimensional (3-D) structures and controllable pore size were fabricated by using microemulsion lyotropic liquid crystal mesophase as templates under acidic conditions. By addition of alkanes with different molecular size (C_6–C_{19} alkyl chains) into the primary lyotropic liquid crystal mesophase of Brij 56 ($C_{16}EO_{10}$), quaternary microemulsion liquid crystal phases formed and the mesophase topology of the surfactant was significantly enhanced with 3-D structures. Hydrocarbon molecular size and the degree of solubilization significantly influenced the amphiphilic phase behavior and the mesopore morphological structure. The phase transitions between the different cubic symmetries could be controlled by using a different solubilizing agent in the microemulsion phases of Brij 56 amphiphile. Thereby, the phase transition of primary liquid crystal mesophases in the microemulsion systems were used to fabricate well-defined highly ordered mesoporous silica monoliths HOM-*n*, including hexagonal *P*6*mm* (HOM-2), 3-D hexagonal $P6_3/mmc$ (HOM-3), primitive-centered cubic *Pn*3*m* (HOM-7), *Pm*3*n* (HOM-9), and *Pm*3*m* (HOM-4) symmetries and body-centered cubic *Im*3*m* (HOM-1), bicontinuous cubic *Ia*3*d* (HOM-5), and face-centered cubic *Fm*3*m* (HOM-10) materials. In these systematic trends, the transitions were primarily governed by the interfacial curvature surface of the amphiphile aggregates. The interactions between alkanes and aggregates substantially influenced the interfacial surface curvatures of micelles, thereby affecting the preferable mesophase structures. However, the primitive cubic (*Pm*3*n*) and face-centered cubic (*Fm*3*m*) monoliths were the most stable phases among all mesophases, indicating that surfaces with high interfacial curvature were obtained by the addition of long hydrocarbon chain lengths (C_{10}–C_{19} range). The addition of short lengths, hexane (C_6) and heptane (C_7), to the aggregate did not significantly affect the shape geometry of the phases, with the exception of the microemulsion lamellar phases formed in the 2-D hexagonal silica monoliths (HOM-2). Our results show that domains with highly curved interfaces were favored in these microemulsion systems. A tailored pore size was obtained within the transition between the 3-D phases with all mesophases. The extent of transition between the phases with enlarged pore dimensions was further studied by varying the amount of solubilizing agent in the microemulsion composition. Large 3-D monoliths of millimeter-sized particles had a wide range of uniform pore size between 30 and 80 Å, high surface area up to 900 m^2/g, and thick walls of about 100 Å. Such properties will allow a wide range of mesoscopic applications.

Introduction

Mesoporous molecular sieves have been synthesized by using amphiphiles as structure-directing agents.[1] In most synthesis strategies, miceller solutions with low surfactant concentrations were used to produce the mesoporous silicates. Three M41S mesophases, namely, MCM-41 (hexagonal *P*6*mm*), MCM-48 (cubic *Ia*3*d*), and MCM-50 (lamellar), have been produced by using ionic surfactants.[1,2] The association and coassembly of the inorganic precursor with an ionic surfactant into the mesophase precipitant are driven by electrostatic interactions between the inorganic ions and surfactant assemblies,[3] and mesophase structural dimensions are controlled by the surfactant length.[4] Nonionic surfactants have been also used to synthesize wormlike disordered mesoporous silica and alumina in neutral media associated by hydrogen-bonding interactions.[5,6]

* Corresponding author. Permanent address: Chemistry Department, Faculty of Science, Tanta University, Tanta-Egypt. Fax: +81-022-2375226, E-mail: Sherif.El-Safty@aist.go.jp or; saes682001@yahoo.co.uk.

† E-mail: hanaoka-takaaki@aist.go.jp.

(1) Kresge, C. T.; Leonowicz, M. E.; Roth, W. J.; Vartuli, J. C.; Beck, J. S. *Nature* **1992**, *359*, 710.

(2) Beck, J. S.; Vartuli, J. C.; Roth, W. J.; Leonowicz, M. E.; Kresge, C. T.; Schmitt, K. D.; Chu, C. T. W.; Olsan, D. H.; Higgins, E. W.; Schlenker, J. L. *J. Am. Chem. Soc.* **1992**, *114*, 10834.

(3) Huo, Q.; Margolese, D. I.; Feng, P. Y.; Gier, T. E.; Stucky, G. D.; Leon, R.; Petroff, P. M.; Ciesla, U.; Schüth, F. *Nature* **1994**, *368*, 317.

(4) Monnier, A.; Schuth, F.; Huo, Q.; Kumar, D.; Margolese, D.; Maxwell, R. S.; Stucky, G. D.; Krishnamurty, M.; Petroff, P.; Firouzi, A.; Janicke, M.; Chmelka, B. F. *Science* **1993**, *261*, 1299.

10.1021/cm034282o CCC: $27.50
Published on Web 01/08/2004

On the other hand, nonionic ethylene oxide surfactants have been used to synthesize highly ordered mesoporous silica materials of SBA families, including 3-D cubic (*Pm*3*m*, *Im*3*m* and *Pm*3*n*), 3-D hexagonal ($P6_3/mmc$), 2-D hexagonal (*P*6*mm*), and lamellar (L_∞) structures.[7−10] Specifically, silica phase structures are controlled by the selected surfactant species. In general, the dilute surfactant solutions have strictly limited the ability to predict the mesophase topologies because the primary phase of the amphiphile is affected by the interactions between the surfactant assemblies and the inorganic precursors. Also, mesoporous powders of micrometer-sized particles (1−2 mm) were produced by applying those synthetic routes.[1−10]

Enlarging the pore size of mesoporous silica materials is being actively researched. For example, triblock poly(ethylene oxide)−poly(propylene oxide)−poly(ethylene oxide) (PEO−PPO−PEO) copolymers have been used as templates to synthesize hexagonal mesoporous silicates SBA-15 with pore sizes from 50 to 300 Å.[11] Among these cubic silicates, SBA-16 (cubic *Im*3*m*) has the largest pore size (54 Å) by synthesis using PEO−PPO−PEO as the template.[10] Large-caged cubic silicate (FDU-1, *Im*3*m*) with pore size of 120 Å has been synthesized with the triblock copolymer PEO−PBO−PEO with a more hydrophobic poly(butylene oxide) as the template.[12] The lyotropic L_3 phase of the surfactant cetylpyridinium chloride was used as a template to form nanoporous monoliths with a pore size of about 6−35 nm.[13] Swelling agents have also been used to expand the pore size by incorporating expanders into the template assemblies to enlarge the volume of micelle via solubilization into the hydrophobic core of aggregates. For example, 1,2,3-trimethylbenzene (TMB) has been used to swell the pores of MCM-41 up to 100 Å.[1,2] Mesostructured cellular foam (MCF) with pore diameter of 22−42 nm was also produced by addition of TMB to PEO−PPO−PEO (P123) template through the phase transition of SBA-15 with cylindrical pore size of 40−120 Å.[14−16] In addition, tetraalkylammonium cations (TAA^+) and hydrocarbon alkanes have been used as expanders, yielding materials with pore sizes larger than 80 Å.[17−20] Although the produced mesoporous silicates had an enlarged pore size, the loss of long-range ordered structures within the arrays often occurred, based on less-resolved X-ray diffraction and broadening of high-intensity signal peaks.

Furthermore, phase transition occurs by adding hydrocarbon auxiliary molecules to aggregate phase assemblies. For example, Su et al.[20] reported that by increasing the TMB or decane auxiliary concentration, MCM-48 can be changed to MCM-41, and with high temperature, MCM-41 can be changed to MCM-48. Stucky et al.[21] reported the phase transition from MCM-41 through MCM-48 to the lamellar phase MCM-50 and concluded that the molecular surfactant packing parameters significantly affect the phase transition and the mesophase structures.[14,21] By using sodium silicate precursors under neutral pH conditions in the microemulsion phase (TMB/P123), Pinnavaia et al. synthesized highly ordered mesoporous silica with large pore structures (MUS-F) analogous to MCF.[22] Kim et al.[23] reported the phase transformation of MCM-41 to hydrothermally stable MCM-48 by direct addition of NaF at 150 °C. Although phase transformation yields materials of enlarged pore size dimensions, the collapse of crystalline mesostructures is often observed with these phase geometrical changes. In addition, large silica monoliths are difficult to obtain within the synthesized materials.

Lyotropic liquid crystalline phases formed at high concentrations of nonionic surfactants (typically 30%) provide a predictable approach for the synthesis of nanocomposite oxides through a direct templating method.[24] The nonionic surfactant, octaethyleneglycol monodecyl ether ($C_{16}EO_8$), has been used to produce three liquid crystalline phases, namely, hexagonal (H_I-silica), cubic (*Ia*3*d*-silica), and lamellar (L_∞-silica).[25] The formation of these mesoporous silicas is independent of the structure and charge of the amphiphiles.[26] The direct templating approach shows promise in fabricating silica monoliths of desired size and shape and in significantly enhancing the control over surfactant phase domains.[27,28] Using Brij 76 ($C_{18}EO_{10}$) as a template, six high-quality silica monoliths (HOM-*n*) have been produced: hexagonal (H_I), lamellar (L_∞), cubic (*Ia*3*d*), cubic (*Im*3*m*), 3-D hexagonal ($P6_3/mmc$), and solid phase (S) materials.[27] Two additional unique liquid crystal phases, namely, cubic *Pn*3*m* and cubic solid phase (*Ia*3*d*) structures, have also been obtained by using Brij 56 as a template.[28] To use these monolithic silicates (HOM-*n*) for applications in optics, electronics, magnetics, filtration, and semiconductors,[29−32] the range of pore sizes must be broadened. However, even in these synthetic

(5) Bagshaw, S. A.; Prouzet, E.; Pinnavaia, T. J. *Science* **1995**, *269*, 1242.
(6) Tanev, P. T.; Pinnavaia, T. J. *Science* **1995**, *267*, 865.
(7) Huo, Q.; Margolese, D. I.; Ciesla, U.; Demuth, D. G.; Feng, P. Y.; Gier, T. E.; Sieger, P.; Leon, R.; Petroff, P. M.; Schüth, F.; Stucky, G. D. *Chem. Mater.* **1994**, *6*, 1176.
(8) Sakamoto, Y.; Kaneda, M.; Terasaki, O.; Zhao, D. Y.; Kim. J. M.; Stucky, G. D.; Shin, H. J.; Ryoo, R. *Nature* **2000**, *408*, 449.
(9) Huo, Q.; Leon, R.; Petroff, P. M.; Stucky, G. D. *Science* **1995**, *268*, 1324.
(10) Zhao, D.; Huo, Q.; Jianglin, F.; Chmelka, B. F.; Stucky, G. D. *J. Am. Chem. Soc.* **1998**, *120*, 6024.
(11) Zhao, D.; Jianglin, F.; Huo, Q.; Melosh, N.; Fredrickson, G. H.; Chmelka, B. F.; Stucky, G. D. *Science* **1998**, *279*, 548.
(12) Yu, C.; Yu, Y.; Miao, L.; Zhao, D. *Microporous Mesoporous Mater.* **2001**, *44*, 65.
(13) McGrath, K. M.; Dabbs, D. M.; Yao, N.; Aksay, I. A.; Gruner, S. M. *Science* **1997**, *277*, 552.
(14) Lettow, J. S.; Han, Y. J.; Schmidt, P.; Yang, P.; Zhao, D.; Stucky, G. D.; Ying, J. Y. *Langmuir* **2000**, *16*, 8291.
(15) Schmidt-Winkel, P.; Lukens, W. W., Jr.; Yang, P.; Margolese, D. I.; Lettow, J. S.; Ying, J. Y.; Stucky, G. D. *Chem. Mater.* **2000**, *12*, 686.
(16) Schmidt-Winkel, P.; Lukens, W. W., Jr.; Zhao, D.; Yang, P.; Chmelka, B. F.; Stucky, G. D. *J. Am. Chem. Soc.* **1999**, *121*, 254.
(17) Corma, A.; Kan, Q.; Navarro, M. T.; Perez-Pariente, J.; Rey, F. *Chem. Mater.* **1997**, *9*, 2123.
(18) Blin, J. L.; Otjacques, C.; Harrier, G.; Su, B. L. *Langmuir* **2000**, *16*, 4229.
(19) Ulagappan, N.; Rao, C. N. R. *Chem. Commun.* **1996**, 2759.
(20) Blin, J. L.; Otjacques, C.; Harrier, G.; Su, B. L. *Stud. Surf. Sci. Catal.* **2000**, *129*, 75.
(21) Huo, Q.; Margolese, D. I.; Stucky, G. D. *Chem. Mater.* **1996**, *8*, 1147.
(22) Kim, S.; Pauly, T. R.; Pinnavaia, T. J. *Chem. Commun.* **2000**, 1661.
(23) Kim, W. J.; Yoo, J. C.; Hayhurst, D. T. *Microporous Mesoporous Mater.* **2001**, *49*, 125.
(24) Attard, G. S.; Glyde, J. C.; Göltner, C. G. *Nature* **1995**, *378*, 366.
(25) Attard, G. S.; Edgar, M.; Göltner, C. G. *Acta Mater.* **1998**, *46*, 751.
(26) Attard, G. S.; Bartlett, P. N.; Coleman, N. R. B.; Elliott, J. M.; Owen, J. R.; Wang, J. H. *Science* **1997**, *278*, 838.
(27) El-Safty, S. A.; Evans, J. *J. Mater. Chem.* **2002**, *12*, 117.
(28) El-Safty, S. A.; Hanaoka, T. *Chem. Mater.* **2003**, *15*, 2892.

Scheme 1. Two Synthetic Pathways for Formation of Mesoporous Silica Monoliths via the Direct Templating Method for Microemulsion Phases

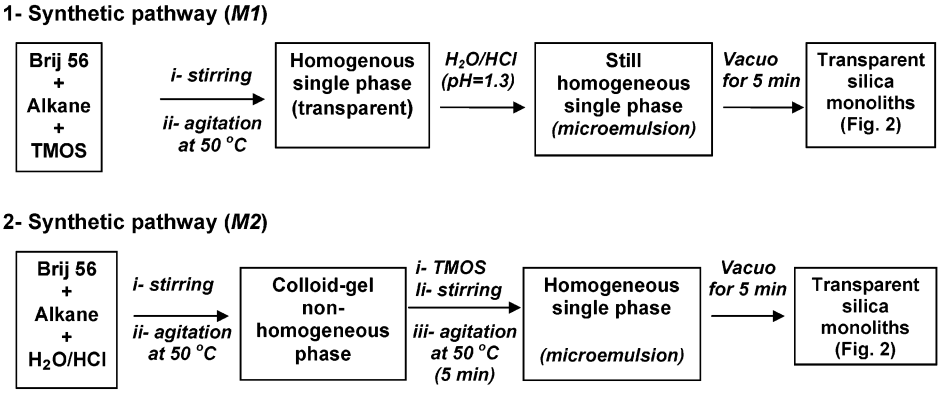

monolithic materials, the pore size is limited to up to 40 Å by the type and composition of the amphiphiles.[24−28]

Here, we developed a simple and versatile methodology that uses microemulsion lyotropic liquid crystal phases of Brij 56 ($C_{16}EO_{10}$) as templates for the synthesis of crystalline silica monoliths (HOM-*n*) with large-caged cubic structures, uniform pore size up to 80 Å, high surface area of 900 m^2/g, and thick walls of 100 Å, yet without the loss of the long-range ordered structures. On the basis of these results, this synthetic methodology revealed new insight into the control of mesophase structural morphology and mesopore organization. This method was successfully used to fabricate well-defined highly ordered HOM-*n* monoliths, such as spherical cubic *Im*3*m* (HOM-1), 3-D hexagonal $P6_3/mmc$ (HOM-3), cubic *Ia*3*d* (HOM-5), cubic *Pn*3*m* (HOM-7), cubic *Pm*3*n* (HOM-9), cubic *Fm*3*m* (HOM-10), and cubic *Pm*3*m* (HOM-4) materials. The phase transitions between these different cubic symmetries represent a significant feature during the synthesis of HOM-*n* monoliths in these microemulsion systems. In addition, the method to fabricate optically transparent macroporous monoliths via the formulation of the true microemulsion liquid crystal phase was significantly discussed. XRD, SEM, and TEM observations and N_2 isotherm absorption/desorption measurements of the synthesized materials revealed that large 3-D HOM-*n* monoliths were credibly synthesized. Such monoliths are in demand for many mesoscopic applications.

Experimental Section

Chemicals. All materials were analytical grade and used as produced without further purification. Tetramethyl orthosilicate (TMOS) and Brij 56 poly(oxyethylene), $C_{16}H_{33}(OCH_2CH_2)_{10}OH$, $C_{16}EO_{10}$) were obtained from Sigma-Aldrich Co. Ltd. The hydrocarbon alkanes with different alkyl chains, such as hexane, heptane, octane, nonane, decane, dodecane, pentadecane, heptadecane, and nonadecane (saturated hydrocarbons, C_nH_{2n+2}), were obtained from Wako.

Sample Syntheses. The microemulsion liquid crystal mesophases were formulated by addition of alkanes (with different alkyl chains of C_6–C_{19} range) into the lyotropic liquid crystal phases of Brij 56 formed at a specific Brij 56/TMOS concentration ratio to form the quaternary system Brij 56/alkane/H_2O−HCl/TMOS. On the basis of a previous report[28] on the synthesis of primary liquid crystal phase topologies used in microemulsion systems, we used a mass ratio of Brij 56:TMOS:H_2O/HCl of 0.7:2:1 for HOM-1 (cubic *Im*3*m*) and 1:2:1 for HOM-2 (hexagonal *P*6*mm*) at 35 °C, 1.36:2:1 for HOM-3 (3-D hexagonal $P6_3/mmc$) and 1.4:2:1 for HOM-5 (cubic *Ia*3*d*) at 45 °C, and 1.5:2:1 for HOM-6 (lamellar L_∞) and 1.7:2:1 for HOM-7 (cubic *Pn*3*m*) at 40 °C. In these six primary phases, the amount of acidified H_2O in the molar ratio of H_2O−HCl/TMOS was about 50 wt %. Also, the mass ratio of Brij 56:alkane was kept constant at 2:1 for all the syntheses of the mesoporous silicates (Tables 2 and 3). Two distinct approaches (respectively designated M1 and M2) of the sol−gel synthesis of the regular silica monoliths (HOM-*n*) are shown in Scheme 1. In both synthetic approaches, stirring and agitation of the initial compositions in a flask at 50 °C were necessary to achieve a homogeneous solution (single phase).

The exothermic hydrolysis and condensation of TMOS were performed quickly in the presence of acidified aqueous/HCl solution at pH 1.3. The methanol produced from the TMOS hydrolysis was removed by using a diaphragm vacuum pump (DIVAC 1.2 L) connected with a rotary evaporator at ambient synthesis temperature to avoid the effect of the destruction of the liquid crystalline order. Within ∼5 min, the resulting viscous liquid changed to an optical gel-like material and acquired the shape and size of the reaction vessel (Figure 2). These translucent birefringent monoliths were collected and dried at 40 °C for 16 h. The surfactant and the incorporated alkanes were removed by calcination at 450 °C (3 h under nitrogen and 14 h under oxygen) for all mesoporous silica structures. The optically birefringent silica monoliths were retained even after drying and removal of the surfactant (Figure 2b).

Analyses. Powder X-ray diffraction (XRD) patterns were measured by using an MXP 18 diffractometer (Mac Science Co. Ltd.) with monochromated Cu Kα radiation. Nitrogen adsorption−desorption isotherms and surface area were measured by using the BET method at 77 K, by using a Shimadzu ASAP 2020 surface area analyzer. All samples were pretreated at 300 °C for 8 h under vacuum until the pressure was equilibrated to 10^{-3} Torr. Transmission electron microscopy (TEM) images were obtained by using a JEOL JEM-2000 FXII operating at an acceleration voltage of 200 kV. The TEM samples were prepared by dispersing the particles onto holey carbon film on a Cu grid. Scanning electron microscopy (SEM) micrographs were obtained by using a Hitachi S-800 SEM operated at 7 keV.

Results and Discussion

1. Formation of Microemulsion Liquid Crystal Phases as Templates. The current design of micro-

(29) (a) Göltner, C. G.; Henke, S.; Weissenberger, M. C.; Antonietti, M. *Angew, Chem. Int. Ed. Engl.* **1998**, *37*, 613. (b) Göltner, C. G.; Antonietti, M. *Adv. Mater.* **1997**, *9*, 431.
(30) Anderson, M. T.; Martin, J. E.; Odinek, J. G.; Newcomer, P. P.; Wilcoxon, J. P. *Microporous Mater.* **1997**, *10*, 13.
(31) Feng, P.; Bu, X.; Stucky, G. D.; Pine, D. J. *J. Am. Chem. Soc.* **2000**, *122*, 994.
(32) Yang, H.; Coombs, N.; Ozin, G. A. *Nature* **1997**, *386*, 692.

emulsion liquid crystal phase included here (Brij 56/alkane/H_2O−HCl) was significantly used as structure-directing agents. The formation of transparent single phase (i.e., true microemulsion phase) was achieved through highly rational solublization of the surfactant/oil/H_2O domains by using the two distinct pathways, M1 and M2 (Scheme 1). By using the M1 approach, TMOS was added to the Brij 56/alkane mixture to promote solublization and could be used as nonaqueous media for maintaining the homogeneity in the synthetic mixture domains. The acidified aqueous solution (H_2O/HCl) was quickly added to the solution domains to immediately form the liquid crystalline phase and to initiate the polymerization of TMOS around the liquid crystal phase (Scheme 2). The rate of polymerization of TMOS was significantly faster (5 min) when microemulsion systems rather than lyotropic phases (10−20 min) were used as a template.[27,28] This faster rate was assumed to be caused by the influence of the hydrophobicity of the alkanes in the core of aggregated micelle during the solublization, as previously discussed.[33] In the M2 pathway, the H_2O−HCl solution was initially added to Brij 56/alkane mixture. A colloid−gel with nonrational solublization (heterogeneity) was clearly evident, particularly with high surfactant concentration, despite continuous stirring and agitation (at 50 °C). However, the acidified solution of HCl yielded certain ions (Cl^-) in the mixture domains, and these ions decreased the solubility of the (EO_{10}) block, as previously reported for triblock copolymer surfactants (PEO−PPO−PEO).[34] By addition of TMOS, the methanol produced from the hydrolysis/condensation reactions of TMOS at the first stage of the synthesis yields well-homogenized phase domains.[29] The M2 pathway could also be preformed by mixing the aqueous solution (H_2O) with the Brij 56/alkane mixture. Despite the presence of the (Cl^-) ions in the initial synthesis domains, the homogeneous solution was clearly formed by addition of TMOS. In this mixture, the ratio between Brij 56:TMOS:H_2O was the same for each phase formed (see the Experimental Section). The polymerization of TMOS around the phase assembly rapidly occurred upon addition of a high concentration of HCl solution at pH = 1 (0.1 mol/L) to the synthetic (Brij 56/alkane/H_2O/TMOS) domains. However, the amount of HCl solution in the HCl:TMOS ratio was about of 15 wt % for all synthesis of mesoporous silica monoliths. By using this synthesis mixture, the monolithic silica structures were typically similar to those of materials fabricated using the M1 approach (Scheme 1), as revealed from the XRD and TEM analyses (Figure 1). This result indicated that no significant changes were evident in the feature of the liquid-crystalline phases of Brij 56 formed by the presence of HCl in mixture domains.

In both sol−gel preparation approaches M1 and M2 of the silica monoliths, the produced methanol eventually destroyed the liquid crystalline phase within the continuous hydrolysis/condensation of the silica precursor (TMOS). Fribreg et al. reported that the role of alcohol (methanol or ethanol) during the hydrolysis of the silicon alkoxides is destruction of the lyotropic

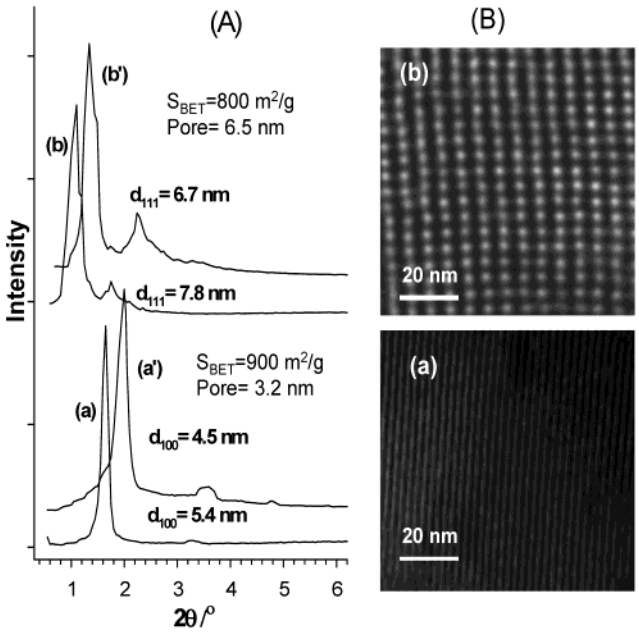

Figure 1. Silica monoliths synthesized using the M2 approach. XRD patterns (A) of (a) as-made and (a′) calcined lamellar L_∞ (HOM-6) synthesized at Brij 56/TMOS at a mass ratio of 75 wt % in a lyotropic system, and of (b) as-made and (b′) calcined cubic *Fm*3*m* (HOM-10) synthesized by addition of dodecane into lamellar phase of Brij 56/TMOS at a mass ratio of 75 wt % in a microemulsion system. TEM images of as-made monolithic silica samples (B) of lamellar phase (a) and cubic *Fm*3*m* phase (b).

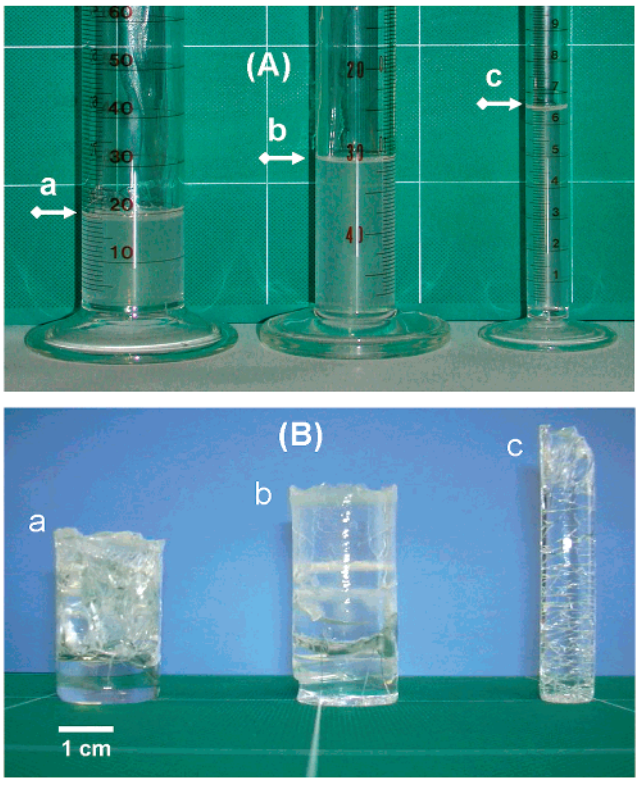

Figure 2. Optically birefringent silica monoliths HOM-*n* with different size and shape. Microemulsion transparent sol−gel as-synthesized monolithic silica of Brij 56 mesophase (A) after gelation and (B) after drying and surfactant removal by ethanol extraction.

liquid-crystalline order in the sol−gel process.[35] Therefore, a gentle vacuum was necessary to remove the

(33) Capek, I.; Juranicova, V.; Barton, J.; Asua, J. M.; Ito, K. *Polym. Int.* **1997**, *43*, 1.
(34) Alexandridis, P.; Holzwarth, J. F. *Langmuir* **1997**, *13*, 6074.

methanol from the Brij 56/TMOS/H_2O mesophase domains. Once the mesophase re-formed, the polymerization silica networks extended throughout the crystalline phase and an optical silica monolithic gel rapidly formed, thus preserving the original phase structure. The formation of transparent homogeneous solution (no turbidity) clearly indicated that the anisotropic feature of the liquid crystalline phase was retained in these microemulsion compositions. Furthermore, in those synthetic methods, our results indicated that the amounts of H_2O and TMOS in the component mixtures were sufficient to form the liquid crystal phases and to fill the aqueous phase domains, respectively, as evidenced by high quality XRD and TEM patterns (as shown in Figures 3−6, discussed in section 3). However, the absence of sufficient amounts of H_2O and TMOS in the synthesis compositions possibly governed the formation of distorted or otherwise unstable mesoporous silica architectures.

No significant changes were evident in the mesoporous silica structures fabricated here by using the synthesis approaches M1 and M2. To generalize the applicability of M1 and M2, we synthesized silica monoliths via the M2 pathway (Scheme 1) in lyotropic and microemulsion (formed with addition of dodecane) liquid crystal phases at the Brij 56/TMOS mass ratio of about 75 wt %, and in the 40−45 °C range. The XRD patterns (Figure 1A) of lamellar L_∞ (HOM-6) and cubic *Fm*3*m* (HOM-10) structures showed well-resolved high order peaks, which were also typically observed in materials synthesized using the M1 pathway (Figures 3 and 11; as discussed in sections 3,7). Interestingly, the *d* spacing values (d_{100} and d_{111}) or the textural parameters (S_{BET} and pore diameter) of lamellar L_∞ and cubic *Fm*3*m* fabricated by using the M2 pathway (Figure 1A) were similar to those of lamellar L_∞ and cubic *Fm*3*m* synthesized by using the M1 pathway (Tables 2 and 3). TEM images (Figure 1B) also revealed that long-range structural ordering was clearly evident in the silica structures synthesized via the M2 pathway. The key result here is that the lamellar L_∞-cubic *Fm*3*m* phase structures in these systems (Figure 1A) were consistent with those phase structures fabricated via the M1 pathway under the same synthetic conditions. This successful fabrication indicates the integrity and feasibility of the *instance preformed phase* (M1) and the *true preformed phase* (M2) pathways to generate high-order monoliths (HOM-*n*).

These provisional results indicate that, for both approaches (M1 or M2), the liquid crystalline phases were significantly maintained so that they can be used as a template. No swelling effect was observed in the produced methanol in the hydrolysis/condensation reaction (Scheme 2) or observed in the prior presence of TMOS in the Brij 56/alkane) mixture domains of the M1 pathway, as evidenced by the texture structural integrity of HOM-*n* monoliths fabricated from M1 and M2 pathways (Figure 1, Table 2). In our synthesis methodology using the M1 and M2 approaches, because conditions are not static during the gelation process, the alcohol or TMOS cannot solubilize in the hydrophobic core of $C_{16}EO_{10}$ species and thus cannot eventually act as swelling agents.[14,36] The major differences between those synthetic pathways are that the M1 approach was characterized by a simple synthesis and by rational solubilizing control over the high composition ratio of Brij 56:TMOS, which governs the feature of the crystalline phases.[28] The use of the M1 pathway solved the difficulty of surfactant solublization and the dehydration effect of HCl addition, particularly with the high molecular weight surfactants (such as di- or triblock copolymer) during the mesoporous silica synthesis. Therefore, the M1 pathway can effectively control the fabrication of mesoporous silica monoliths at high surfactant concentration up to 90 wt %. Furthermore, the agitation and stirring for 5 min (Scheme 1) to achieve homogeneity of the mixture (Brij 56/alkane/H_2O−HCl) domains via M2 pathway after addition of TMOS might "melt" the crystalline phases formed, although the phase behavior of nonionic surfactant ($C_{16}EO_{10}$) is highly dependent on temperature.[28] Kunieda et al. also reported that by increasing the temperature, the hexagonal liquid crystal phase formed with nonionic surfactant $C_{12}EO_7$/water domains could be melted to form aqueous micellar solution.[37] These results indicate that the fabrication of the mesoporous silica monoliths via the M1 pathway methodology can be generalized for all synthesis systems.

2. Monolithic Silica (HOM-*n*) Fabricated by Microemulsion Systems. In these microemulsion systems, rapid gelation (∼5 min) and formation of the glassy mesoporous silica were achieved by using strong acid (pH ∼1) as a condensation catalyst. Control of the rate and extent of the hydrolysis/condensation reactions of the silica precursors is influenced by the nature of the additive medium, pH of the solution, temperature, H_2O:alkoxide ratios, and catalysts into the phase domains.[9,10] Boissiére et al. reported that the formation of powder MSU-X mesoporous silica could be produced through a two-step synthesis, namely, the assembly of the silica oligomers around the micelles and then condensation with addition of NaF as catalyst.[38] In acid-catalyzed synthesis, the hydrolysis/condensation reactions of the alkoxsilanes (TMOS) in the microemulsion liquid crystal phases can be summarized as such a two-step synthesis (Scheme 2).[10]

Note that in our synthesis, TMOS hydrolyzed at low pH ∼1 formed positively charged protonated silica species (≡$Si(OH_2)^+$) and methanol. These silica species were the only intermediate species to form siloxane

Scheme 2. Silica Polymerization in Sol−Gel Microemulsion Systems

1- Hydrolysis

$$(CH_3O)_3\text{-Si-}OCH_3 + H_2O \xrightarrow{H^+} (MeO)_3\text{-Si}OH_2^+ + CH_3OH$$

2- Condensation

$$(MeO)_3\text{-Si}OH_2^+ + MeO\text{-Si-} \longrightarrow \text{-(-Si-O-Si-)}_n\text{-} + CH_3OH$$

$$(MeO)_3\text{-Si-OH} + HO\text{-Si-} \longrightarrow \text{-(-Si-O-Si-)}_n\text{-} + H_2O$$

Table 1. Representative Silica Monoliths HOM-*n* Structures Synthesized in Microemulsion Systems Formed with Addition of Oils (Alkyl Chains with C_6–C_{19}) into Six Lyotropic Mesophases of Brij 56

primary lyotropic mesophases[a]	monolithic silica structures synthesized in microemulsion systems with additive alkanes						
	C_6, C_7	C_8	C_9	C_{10}	C_{12}	C_{15}	C_{17}–C_{19}
cubic *Im*3*m*	cubic *Im*3*m*	cubic *Pm*3*n*	cubic *Pm*3*n*	cubic *Pm*3*n*	cubic *Pm*3*n*	cubic *Pm*3*n*	cubic *Pm*3*n*
hexagonal *P*6*mm*	hexagonal *P*6*mm*	3-D hexagonal $P6_3/mmc$	cubic *Pm*3*n*	cubic *Pm*3*n*	cubic *Pm*3*n*	cubic *Pm*3*n*	cubic *Pn*3*m*
3-D hexagonal $P6_3/mmc$	3-D hexagonal $P6_3/mmc$	3-D hexagonal $P6_3/mmc$	cubic *Im*3*m*	cubic *Fm*3*m*	cubic *Fm*3*m*	cubic *Fm*3*m*	cubic *Fm*3*m*
cubic *Ia*3*d*	cubic *Ia*3*d*	cubic *Ia*3*d*	cubic *Im*3*m*	cubic *Fm*3*m*	cubic *Fm*3*m*	cubic *Fm*3*m*	cubic *Fm*3*m*
lamellar L_∞	hexagonal *P*6*mm*	cubic *Im*3*m*	cubic *Pm*3*m*	cubic *Fm*3*m*	cubic *Fm*3*m*	cubic *Fm*3*m*	cubic *Fm*3*m*
cubic *Pn*3*m*	cubic *Pn*3*m*	cubic *Pn*3*m*	cubic *Pn*3*m*	cubic *Pn*3*m*	cubic *Pm*3*n*	cubic *Pm*3*n*	cubic *Fm*3*m*

[a] These materials were synthesized by using lyotropic phases as template.[28]

(Si−O−Si) in the subsequent condensation. As the hydrolysis and condensation continued, viscous gel-like materials formed via the evacuation of the methanol. Therefore, the silica networks were extended around the crystalline phase to form surfactant−silica hybrid structures. The hydrophilic (EO) units of Brij−surfactant ($C_{16}EO_{10}$) in the bulk microemulsion lyotropic phase interacted with silica intermediate species through hydrogen-bonding or weak electrostatic interactions to promote the self-assembly of the silica−surfactant mesophase gel. Large monoliths were successfully fabricated, even in the absence of the strong interaction between surfactant/silica oligomers, indicating that the formation of monoliths does not depend on the type of interaction or the surfactant structural charge.[39]

The key result in our study is the formation of translucent, not opaque, anisotropic monoliths with these microemulsion systems, as shown in Figure 2. After the removal of the Brij 56 surfactant, the transparent monoliths clearly had stable birefringent structures of the macroscopic cylindrical-like particles with different size (Figure 2b). However, because these synthetic monoliths were preformed in dry air without care and caution, cracks appeared.[29] Despite the cracks, the strength and toughness of the transparent structures have been retained for at a least 1 year (the first fabrication of these materials was preformed 1 year to date). Crystalline materials, with their arrangements of atoms, are naturally birefringent (i.e., defined as the dependence of refractive index on polarization direction[40]) and have anisotropic optical properties, particularly with the 1-D lamellar and 2-D hexagonal phase structures. Due to the constraints by their high symmetry, certain classes of crystalline materials with cubic symmetry of their crystal lattice are isotropic and nonbirefringent, at least in the lowest order.[40] Therefore, the crystalline cubic HOM-*n* monoliths fabricated in our study had a highly ordered arrangement of atoms in the cubic crystal lattice, as clearly evident in the XRD patterns and TEM images (Figures 3−6). This crystalline feature might have induced the birefringence of these monolithic materials. However, further study is needed to verify that these HOM-*n* monoliths exhibit birefringent properties.

3. Characterization of Mesoporous Monolithic Silica Structures. In a previous study, we reported that this direct templating methodology in bulk lyotropic liquid crystal phases of Brij 56 can successfully fabricate six highly ordered silica monoliths (HOM-*n*) with 3.0−3.5 nm pore dimension.[28] The monolithic structures included 1-D lamellar L_∞ (HOM-6), 2D hexagonal *P*6*mm* (HOM-2), 3D hexagonal $P6_3/mmc$ (HOM-3), and 3-D accessible cubic *Im*3*m* (HOM-1), *Ia*3*d* (HOM-5), and *Pn*3*m* (HOM-7) materials (Tables 1 and 3). In our current study, to investigate the effect of the additive alkanes as cosolvent to the Brij 56 phases in the quaternary microemulsion systems, we used the synthetic M1 approach with the six lyotropic liquid crystal phases of Brij 56 at the same ambient compositions, temperatures, and pH. In these systematic microemulsion designs, the addition of alkanes with various hydrocarbon molecular sizes (C_6–C_{19} alkyl chain range) and degree of solubilization significantly influenced the amphiphilic phase behavior and the mesopore morphological structure. The synthesis of large silicate monoliths over a wide range of pore sizes with significant order of materials was feasibly achieved (Tables 2−4). In the microemulsion systems fabricated here, the aggregate reassemblies depended on the nature of the interactions between the solubilizing agent and structure block lengths of Brij 56 species (hydrophobic length, C_{16}, and hydrophilic length, EO_{10}), as shown in Scheme 4. Surprisingly, the incorporation of the alkanes into the defined primary phase of surfactant aggregate affected the interfacial curvature, and this curvature might determine the preferred cubic symmetry lattice. Therefore, the formation of HOM-*n* silica monoliths occurred throughout the phase transitions between the different microemulsion lyotropic mesophase topologies of Brij 56 (Table 1). Monolithic 3-D HOM-10 (cubic *Fm*3*m*), HOM-4 (cubic *Pm*3*m*), and HOM-9 (cubic *Pm*3*n*) structures were only fabricated in these microemulsion systematic designs, suggesting a significant influence of the alkane interactions on the amphiphile phase behavior. Furthermore, the mesoporous silica monoliths, such as HOM-1 (cubic *Im*3*m*), HOM-3 (3-D hexagonal $P6_3/mmc$), HOM-5 (cubic *Ia*3*d*), HOM-7 (cubic *Pn*3*m*), and HOM-2 (2-D hexagonal *P*6*mm*), were fabricated in lyotropic and microemulsion phases (Table 1) with enlarged pore sizes depending on the alkyl chain lengths of the solubilizing agents (Tables 2−4). Note that in our synthesis, lamellar (L_∞) silica monoliths (HOM-6) were only synthesized

(35) (a) Friberg, S. E.; Yang, C. C.; Goubran, R.; Partch, R. E. *Langmuir* **1991**, *7*, 1103. (b) Friberg, S. E.; Yang, C. C.; Sjöblom, J. *Langmuir* **1992**, *8*, 372.
(36) Blin, J. L.; Becue, A.; Pauwels, B.; Van Tendeloo, G.; Su, B. L. *Microporous Mesoporous Mater.* **2001**, *44*−*45*, 41.
(37) Kunieda, H.; Umizu, G.; Aramaki, K. *J. Phys. Chem. B* **2000**, *104*, 2005.
(38) Boissiére, C.; Larbot, A.; Bourgaux, C.; Prouzet, E.; Bunton, C. A. *Chem. Mater.* **2001**, *13*, 3580.
(39) El-Safty. S. A. *J. Colloid Interface. Sci.* **2003**, *260*, 184.
(40) (a) Agranovich, V.; Ginzburg, V. *Crystal Optics with Special Dispersion and Excitons*, 2nd ed.; Springer-Verlag: New York, 1984. (b) Burnett, J.; Levine, Z. *Phys. Rev. B* **2001**, *64*, 241102.

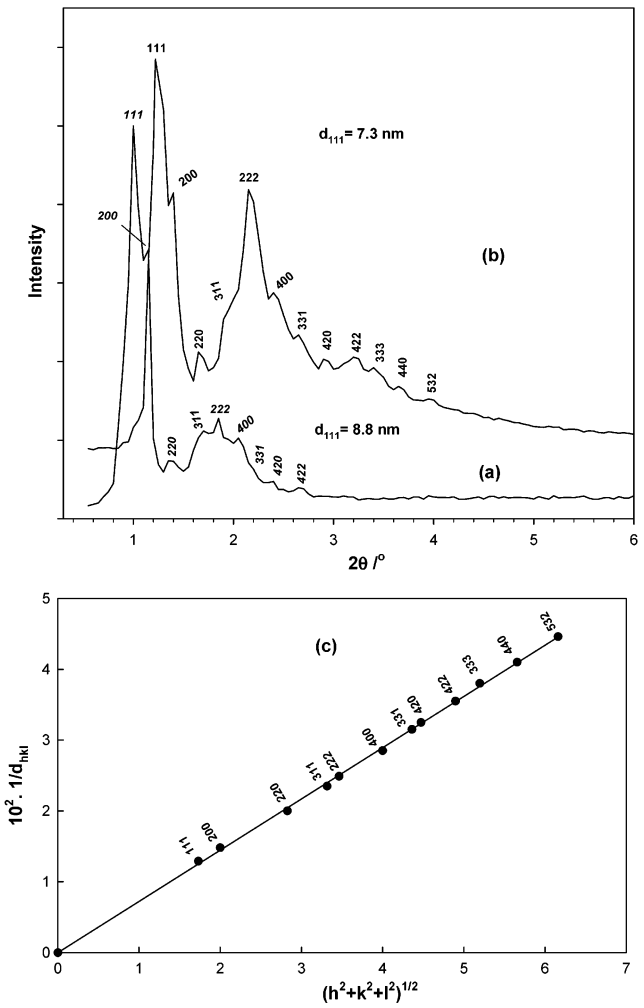

Figure 3. XRD patterns of silica monoliths. (a) As-made and (b) calcined cubic *Fm*3*m* (HOM-10) synthesized by incorporating pentadecane into the 3-D hexagonal phase of Brij 56/TMOS at a mass ratio of 69 wt % in a microemulsion system. (c) Representative plot of $1/d_{hkl}$ vs $(h^2 + k^2 + l^2)^{1/2}$ for all assigned X-ray diffraction *hkl* of calcined HOM-10.

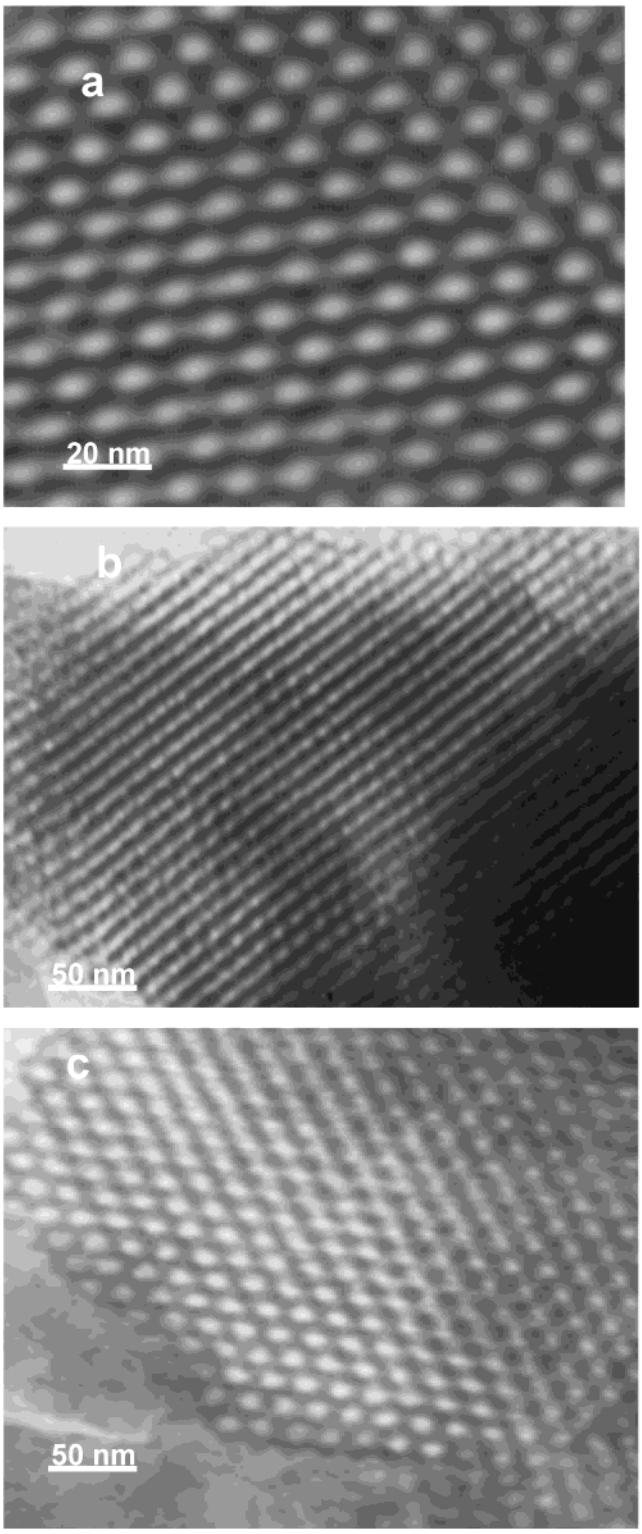

Figure 4. Representative TEM images of monolithic silica viewed along the (a) [100], (b) [111], and (c) [110] directions of cubic *Fm*3*m* (HOM-10) samples synthesized by incorporating decane into the cubic *Ia*3*d* phase of Brij 56/TMOS at a mass ratio of 70 wt % in microemulsion liquid crystal.

by using the lyotropic liquid crystal phase of Brij 56 at 75 wt % ratio as template (Figure 1, Table 3).[28] Our results show that the formation of periodic silica monoliths HOM-*n* using the direct templating microemulsion liquid crystal regime is a desirable additional route for controlling the synthesis of large-pore morphology of the 3-D materials.

3.1. HOM-n Monoliths Formed with Microemulsion Systems via Phase Transition.

3.1.1. Fm3m Cubic Structure (HOM-10). One of the most significant results in our study was the successful fabrication of high-quality cubic *Fm*3*m* mesoporous silicas (HOM-10) by using microemulsion lyotropic liquid crystal under high concentrations (Brij 56/TMOS) between 69% and 85% (w/w) over a wide range of additive long alkyl chain length (C_{10}–C_{19}). The exception was the cubic *Pn*3*m* phase of 85 wt % Brij 56/TMOS ratio used with the range of additive C_{17}–C_{19} alkyl chains. The XRD pattern of an as-synthesized sample of HOM-10 (Figure 3a) showed two strong reflections with *d* spacing 88.3 and 77.0 Å, which are indicative of (111) and (200) reflections, respectively. Several well-resolved reflections in the $1.4° \leq 2\theta \leq 2.7°$ range were also observed. Such systematic Bragg reflections were bulk-resolved, clearly indicating a distinctive topological change in primary mesophase.

After calcination, the diffraction peaks were still observed at high intensity with reduced *d* spacing (Figure 3b), suggesting that shrinkage of the HOM-10 lattice structures occurred during the high-temperature

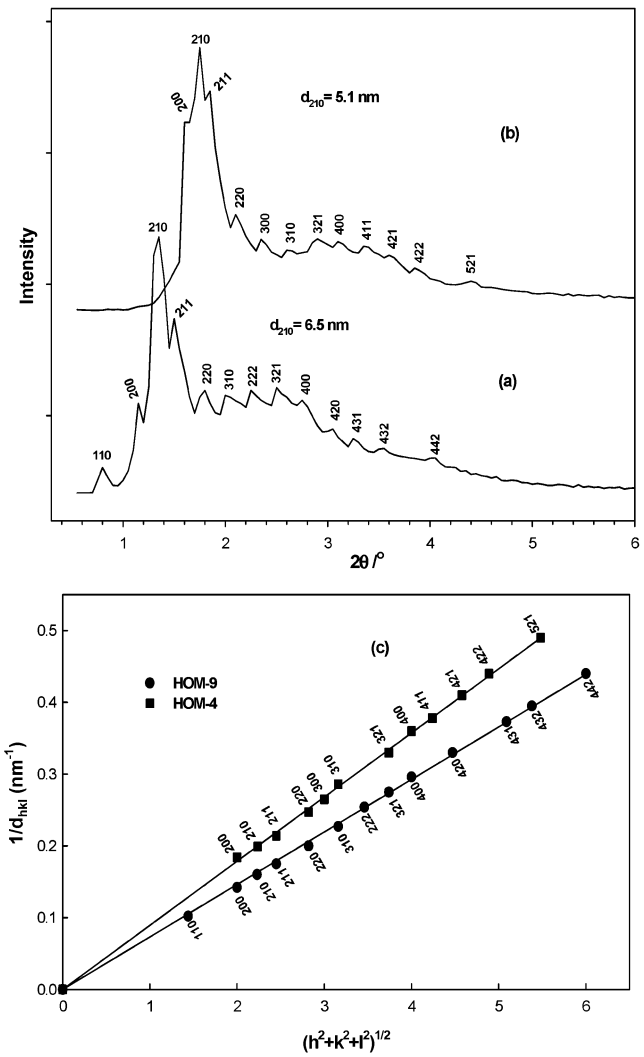

Figure 5. XRD patterns of mesoporous silica materials of (a) cubic *Pm*3*n* (HOM-9) synthesized by incorporating dodecane into primary the cubic *Pn*3*m* phase of Brij 56/TMOS at a mass ratio of 85 wt % and (b) cubic *Pm*3*m* (HOM-4) synthesized by incorporating nonane into lameller (L_∞) phase of Brij 56/TMOS at a mass ratio of 75 wt %. (c) Representative plot of $1/d_{hkl}$ vs $(h^2 + k^2 + l^2)^{1/2}$ for all assigned X-ray diffraction *hkl* of HOM-9 and HOM-4.

treatment at 450 °C. The shrinkage was mainly due to the loss of the organic template and to the densification of the silica wall by the condensation of silanol groups.[2,34] Well-resolved XRD peaks appeared in the region $1.2° \leq 2\theta \leq 4°$, consistent with a face-centered cubic symmetry, space group *Fm*3*m*.[41] In addition, the diffractions of cubic *Fm*3*m* phase domains were characterized by the unique and sharp (222) plane (Figure 3b), clearly indicating the crystallinity of the HOM-10 monoliths. The high-intensity (111) peak indicates a large unit-cell dimension a_o ($=d_{111}\sqrt{3}$) between 106 and 129 Å, suggesting a large-caged cubic *Fm*3*m* mesostructure (Table 2). The diffraction data revealed the formation of thermally stable cubic *Fm*3*m* structures through the phase transition of the liquid crystal 3-D hexagonal $P6_3/mmc$, cubic *Ia*3*d*, lamellar (L_∞), and cubic *Pn*3*m* phases, reflecting the high degree of control over the mesopore organization of materials. This HOM-10 phase might

Table 2. Structural Parameters of HOM-*n* Mesoporous Silica Monoliths Synthesized in Microemulsion Systems: Unit Lattice Dimension (a_o), BET Surface Area (S_{BET}), Pore Size (R), and Wall Thickness (W)

HOM-*n* monolith	cubic structure	Brij56/ TMOS,[a] %	alkyl chain length	*T*, °C	a_o, Å	S_{BET}, m^2/g	*R*, Å	*W*, Å
HOM-10	*Fm*3*m*	69	C_{10}	45	109	688	60	49
		69	C_{12}	45	128	731	70	58
		69	C_{15}	45	126	777	70	55
		69	C_{17}	45	128	682	71	57
		69	C_{19}	45	123	704	62	61
		70	C_{10}	45	106	739	59	47
		70	C_{12}	45	129	674	72	57
		70	C_{15}	45	119	860	63	56
		70	C_{17}	45	118	877	60	58
		70	C_{19}	45	115	826	64	51
		75	C_{10}	40	106	762	59	47
		75	C_{12}	40	114	765	65	47
		75	C_{15}	40	118	850	68	50
		75	C_{17}	40	106	800	63	43
		75	C_{19}	40	106	765	57	49
		85	C_{17}	40	120	856	72	48
		85	C_{19}	40	119	830	70	48
HOM-9	*Pm*3*n*	35	C_8	35	124	665	38	86
		35	C_9	35	129	677	39	90
		35	C_{10}	35	130	694	41	89
		35	C_{12}	35	136	615	47	89
		35	C_{15}	35	120	642	40	80
		35	C_{17}	35	113	656	36	77
		35	C_{19}	35	111	657	35	76
		50	C_9	35	136	680	46	90
		50	C_{10}	35	146	658	53	93
		50	C_{12}	35	152	695	61	91
		50	C_{15}	35	133	756	53	80
		85	C_{12}	40	145	760	71	74
		85	C_{15}	40	150	740	76	74
HOM-4	*Pm*3*m*	75	C_9	40	114	790	46	68

[a] This refers to [wt of Brij 56/wt of TMOS] × 100.

be synthesized at the largest surface curvature of globular aggregates, depending on the degree of penetration of alkanes into the micelle aggregate species.[41]

The good fit of the linear plot of $1/d_{hkl}$ vs $(h^2 + k^2 + l^2)^{1/2}$ (Figure 3c) for the distinguishable diffraction peaks of cubic *Fm*3*m* monoliths (Figure 3b) indicates the high order of cubic *Fm*3*m* structures.[42] Figure 4 shows TEM images of the lattice of HOM-10 cubic *Fm*3*m* silica monoliths recorded along the [100], [111], and [110] directions of the mesostructures. The TEM image in the [100] direction (Figure 4a) reveals the well-defined and regular mesopore structures of such *Fm*3*m* cubic symmetry. The image in the [111] direction confirms the significant long-range uniform channel system. The image in the [110] direction reveals well-oriented channels arranged along [110] directional arrays. The overall TEM lattice images reveal the contribution of the formation of the highly ordered cubic mesoporous silica with face-centered *Fm*3*m* symmetry.

3.1.2. Pm3n Cubic Structure (HOM-9). In the phases observed at low Brij 56/TMOS concentration ratios of 35 wt % (cubic *Im*3*m*) and 50 wt % (hexagonal *P*6*mm*), cubic *Pm*3*n* structure (HOM-9) was the predominant phase formed in microemulsion systems with additive alkanes in the range of C_9–C_{15} alkyl chains. HOM-9 was also observed in the microemulsion cubic *Pn*3*m* (85 wt %) phase with additive alkanes in the range of C_{12}–C_{15}

(41) Maddaford, P. J.; Toprakcioglu, C. *Langmuir* **1993**, *9*, 2868.

(42) Mariani, P.; Luzzati, V.; Delacroix, H. *J. Mol. Biol.* **1988**, *204*, 165.

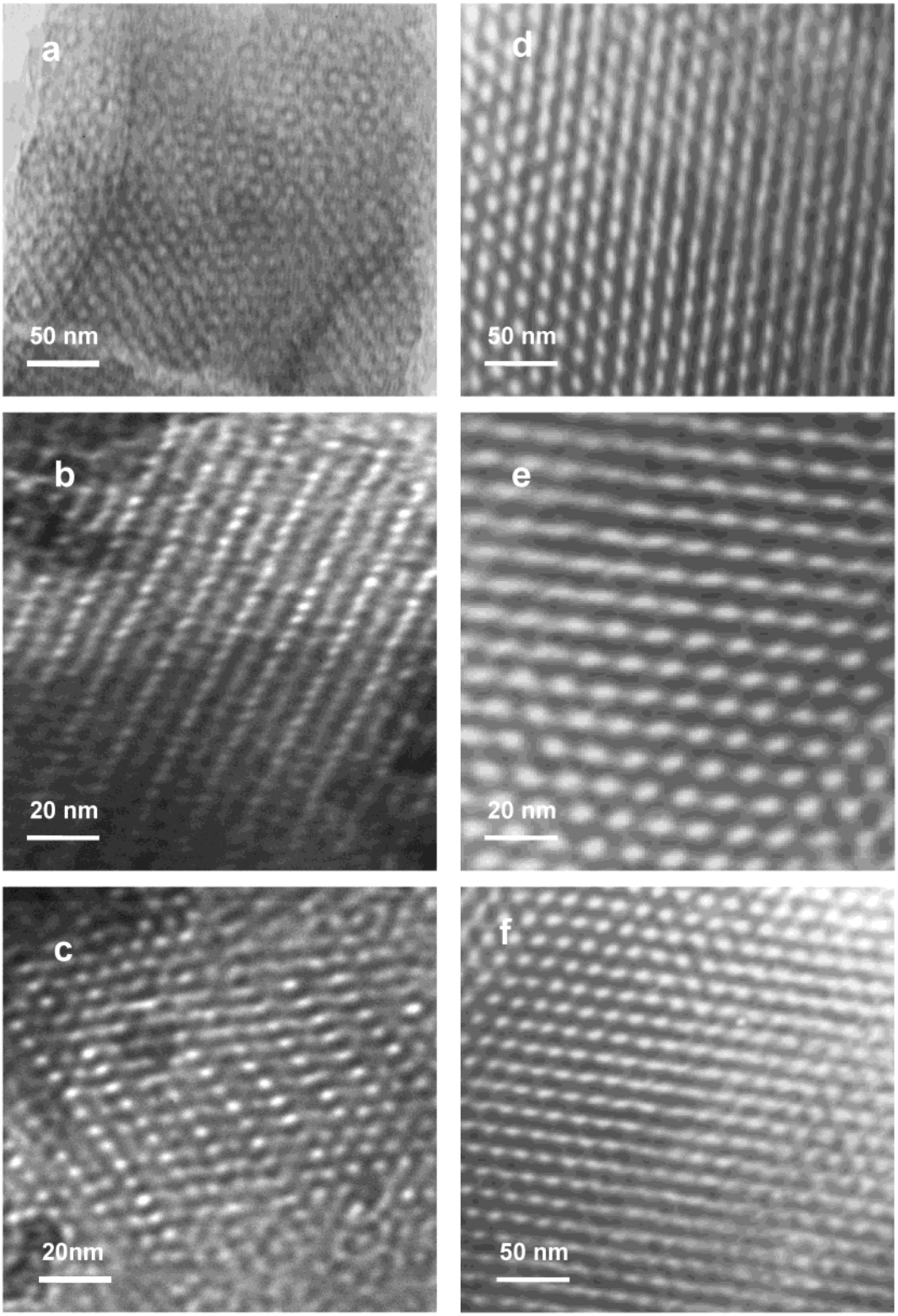

Figure 6. Representative TEM images of mesoporous silica monoliths. Viewed along the (a) [100], (b) [110], and (c) [210] directions of cubic *Pm*3*n* (HOM-9) synthesized by incorporating dodecane into cubic *Im*3*m* liquid crystal phase of Brij 56/TMOS at a mass ratio of 35 wt %. Viewed along the (d) [111], (e) [110], and (f) [100] directions of cubic *Pm*3*m* (HOM-4) synthesized by incorporating nonane into lamellar liquid crystal phase of Brij 56/TMOS at a mass ratio of 75 wt %.

alkyl chains (Table 1). The XRD pattern of HOM-9 (Figure 5a) shows evidence of a unique signal at low 2θ angle (<1°), which can be assigned to (110) refraction, and three well-resolved peaks in the range $1° \leq 2\theta \leq 2°$, respectively assigned to (200), (210), and (211) diffractions, for the cubic crystallographic *Pm*3*n* structure.[8] The intensity and resolution of all reflections strongly reflect a high degree of 3-D architecture ordering, consistent with the reported mesoporous SBA-1 of cubic *Pm*3*n* phase.[8,43] The high intensity (210) peak of the HOM-9 monoliths produced a large a_o in the 129−152 Å range (Table 2), which depended on the nature

Table 3. Structural Parameters of HOM-*n* Mesoporous Silica Monoliths Synthesized in Both Lyotropic and Microemulsion Systems: Unit Lattice Dimension (a_o), BET Surface Area (S_{BET}), Pore Size (R), and Wall Thickness (W)

HOM-*n* monolith	mesoporous structure	Brij56/ TMOS, %	alkyl chain length	T, °C	a_o, Å	S_{BET}, m^2/g	R, Å	W, Å
HOM-1	cubic *Im*3*m*	35	—[a]	35	65	690	32	33
		35	C_6	35	66	727	33	33
		35	C_7	35	68	709	34	34
		69	C_9	45	85	900	48	37
		70	C_9	45	92	794	48	44
		75	C_8	40	69	845	40	25
HOM-3	3-D hexagonal *P*6$_3$/*mmc*	69	—	45	88	828	34	54
		69	C_6	45	88	822	34	54
		69	C_7	45	90	846	36	55
		69	C_8	45	91	850	38	53
		50	C_8	35	110	635	42	68
HOM-5	cubic *Ia*3*d*	70	—	45	103	832	32	71
		70	C_6	45	105	847	35	70
		70	C_7	45	107	944	37	70
		70	C_8	45	109	844	39	70
HOM-7	cubic *Pn*3*m*	85	—	40	100	837	30	70
		85	C_6	40	103	863	33	70
		85	C_7	40	106	850	36	70
		85	C_8	40	113	920	40	73
		85	C_9	40	130	890	42	88
		85	C_{10}	40	154	720	46	108
		50	C_{17}	35	144	655	47	97
		50	C_{19}	35	127	651	42	85
HOM-2	2-D hexagonal *P*6*mm*	50	—	35	55	800	32	23
		50	C_6	35	55	710	35	20
		50	C_7	35	56	655	37	19
		75	C_6	40	54	875	34	12
		75	C_7	40	55	890	37	11
HOM-6	lamellar L_∞	75	—	40	46	810	32	14

[a] Samples were synthesized using lyotropic liquid crystal phase as template.[28]

Table 4. Effect of the Amount of Additive Alkane (Dodecane) on the Mesophase Structure of Mesoporous Silicates Synthesized by Using Hexagonal Microemulsion Liquid Crystal Phase Template: Unit-Cell Parameter (a_o), Surface Area (S_{BET}), Pore Diameter (R), and Wall Thickness (W)

molar ratio of Brij56:alkane	mesoporous silica structure	a_o, Å	S_{BET}, m^2/g	R, Å	W Å
1:0.0	hexagonal *P*6*mm*	55	800	32	23
2:0.25	hexagonal *P*6*mm*	60	773	36	24
2:0.5	cubic *Pm*3*n*	132	704	46	86
4:1.5	cubic *Pm*3*n*	146	670	54	92
2:1.0	cubic *Pm*3*n*	152	695	61	91
4:3.0	cubic *Pm*3*n*	141	698	54	87
1:1.0	cubic *Pm*3*n*	136	625	48	88
1:2.0	cubic *Pm*3*n*	127	635	45	82
1:3.0	cubic *Pm*3*n*	125	704	40	85

of the alkane interactions with the hydrophobic−hydrophilic interface of the micelle aggregate in each lyotropic phase.[44,45]

The TEM image of HOM-9 cubic *Pm*3*n* along the [100] direction (Figure 6a) revealed well-defined edges with a spherical shape, indicating the cubic *Pm*3*n* symmetry.[8] The image along the [110] direction (Figure 6b) revealed uniform mesopore channels of 3-D cubic *Pm*3*n* structures. The image along the [210] direction (Figure 6c) revealed regular straight arrays running along a large area of this direction. The well-defined white dots along the channels confirmed the [210] orientation.[3] The estimated a_o along the [210] direction was about 140 Å, which agrees well with the a_o determined from X-ray diffraction of HOM-9 (Table 2).

3.1.3. Pm3m Cubic Structure (HOM-4). The XRD pattern of cubic *Pm*3*m* lattice (HOM-4) (Figure 5b) prepared in the microemulsion lamellar phase of Brij 56 (75 wt %) with nonane (C_9) reveals three poorly defined high-intensity peaks at $1° \leq 2\theta \leq 2°$ with respective d spacing ratios of $\sqrt{4}:\sqrt{5}:\sqrt{6}$. These XRD diffraction planes indicate the long-range order of cubic *Pm*3*m* mesoporous silica with $a_o = 114$ Å (Table 2). In a previous study, cubic *Pm*3*m* symmetry (SBA-11) was prepared by using $C_{16}EO_{10}$ species under acidic conditions with small pore size (2.5 nm diameter).[10] In our current study, based on the well-resolved XRD pattern (Figure 5b), highly ordered, crystalline cubic *Pm*3*m* structures were successfully fabricated in the microemulsion lamellar liquid crystal. The straight line passing through the origin of the $(1/d_{hkl})$ vs $(h^2 + k^2 + l^2)^{1/2}$ plot indicates the integrity of primitive-centered cubic mesoporous structures with *Pm*3*n* and *Pm*3*m* space groups (parts c and d of Figure 5, respectively).

The TEM images of HOM-4 reveal well-ordered mesopores along the [111] and [110] directions (Figure 6d,e), suggesting a precise order of 3-D cubic *Pm*3*m* mesopore architectures.[10] The image along the [100] direction (Figure 6f) reveals uniform channels of HOM-4 cubic *Pm*3*m* lattice. The distance between these channels in the [100] direction was about 4.9 nm, agreeing with the d_{210} X-ray diffraction plane.

3.2. HOM-n Monoliths Synthesized with Microemulsion and Lyotropic Systems. The HOM-7 cubic *Pn*3*m* structure was successfully synthesized with addition of heptadecane (C_{17}) and nonadecane (C_{19}) in the microemulsion composition of hexagonal phase (50 wt %). This monolithic surfactant/silica phase (cubic *Pn*3*m*) preserved a large degree of structural stability in the microemulsion lyotropic phase at 85 wt % of Brij 56 formulated with additive C_6−C_{10} alkyl chains. The XRD pattern showed two high quality peaks at low 2θ (<1°) and three well-resolved reflection peaks, similar to those previously reported for HOM-7 materials fabricated in the absence of the microemulsion systems (see Supporting Information, Figure 1S).[28] The XRD pattern also showed high-resolution peaks in in the region $1.8° \leq 2\theta \leq 4.2°$, which are expected for a high-order *Pn*3*m* cubic liquid crystalline mesophase with lattice constants up to 154 Å (Table 3).[46] In fact, the interaction between alkanes and the interior aggregates of cubic *Pn*3*m* mesophase enhances the control over the cubic *Pn*3*m* mesopore organization, as evidenced by the retention of the high-order XRD pattern for the cubic *Pn*3*m* crystallographic structure.

The XRD pattern revealed cubic *Ia*3*d* mesophase (HOM-5) derived with additive hydrocarbon C_7 and C_8 alkyl chains in a microemulsion system of liquid crystal cubic *Ia*3*d* phase (70 wt %). These HOM-5 samples had high-quality reflection peaks from (211) to (543) planes

(43) Zhao, D.; Yang, P.; Margolese, D. I.; Chmelka, B. F.; Stucky, G. D. *Chem. Commun.* **1998**, 2499.
(44) Attard, G. S.; Fuller, S.; Howell, O.; Tiddy, G. J. T. *Langmuir* **2000**, *16*, 8712.
(45) Kunieda, H.; Ozawa, K.; Huang, K. *J. Phys. Chem. B* **1998**, *102*, 831.
(46) Honma, I.; Zhou, H. S.; Kundu, D.; Endo, A. *Adv. Mater.* **2000**, *12*, 1529.

Scheme 3. Phase Transition Sequence between Mesoporous Silica Structures (HOM-*n*) in These Microemulsion Systems[a]

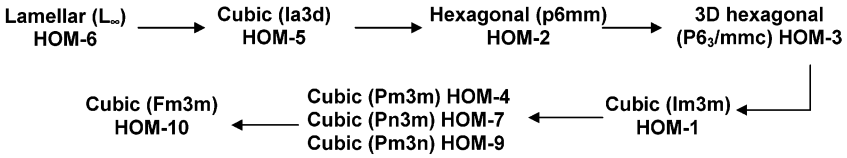

[a] (i) Sequence of these structure changes include the effect of additive alkane in all primary lyotropic liquid crystal phases of Brij 56 (Table 1). (ii) The direction of the arrow indicates the preferable phase transition in these systems.

Scheme 4. Feasibility of Solubilization of Alkane into Brij 56 ($C_{16}EO_{10}$) Surfactant Layers

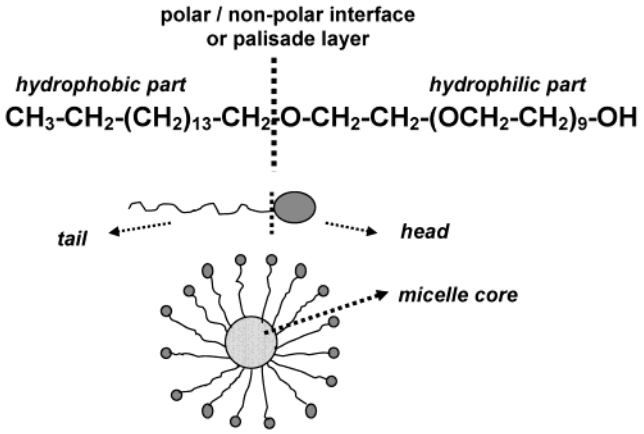

(see Supporting Information, Figure 1S).[2,27] The a_o (Table 3) slightly increased with increasing chain length of the additive hydrocarbon, suggesting the dispersion of alkane molecules between the surfactant micellar aggregates (see Scheme 4).[19] The stability of the cubic *Ia*3*d* structure might be attributed to the relative ineffectiveness of the hydrocarbon molecules of C_6 to C_8 alkyl chains to change the curved aggregates arranged in the cubic *Ia*3*d* phase structure. This stability of phase behavior is similar to that in the synthesis of the 3-D hexagonal $P6_3/mmc$ (HOM-3) in microemulsion liquid crystal phase with addition of hydrocarbon molecules of C_6 to C_8 alkyl chains to primary 3-D hexagonal (69 wt %) phase (Table 3). Despite this phase behavior, the addition of octane (C_8 alkyl chain) into hexagonal *P*6*mm* (50 wt %) phase led to the formation of the HOM-3 mesostructures, which are indicative of the greater surface curvature of organized 3-D hexagonal $P6_3/mmc$ compared with that of 2-D hexagonal *P*6*mm* (Table 1) phase. The XRD pattern showed highly ordered diffraction peaks of 3-D hexagonal $P6_3/mmc$ mesophase with ideal unit cell dimensions of a_o= 67.9 Å, c = 110.4 Å, c/a_o = 1.62, as previously reported (see Supporting Information, Figure 2S).[9,27] In conclusion, the penetration of octane into the micelle assembly of the hexagonal mesophase induced the formation of 3-D hexagonal $P6_3/mmc$ mesoporous silicate, derived from a hexagonal close packing of globular aggregate structures.[10] Furthermore, the molecular size of the alkanes strongly affected the phase transition determination of the cubic *Im*3*m* mesopore organization (HOM-1). However, HOM-1 monoliths were fabricated in microemulsion systems of cubic *Ia*3*d* (70 wt %) and 3-D hexagonal (69 wt %) phase with additive nonane and of lamellar (75 wt %) phase with additive octane (Table 1). The XRD pattern of HOM-1 showed reflection peaks that are indicative of a significantly higher degree of crystallinity and textural uniformity over the 3-D channel of cubic *Im*3*m* networks (see Supporting Information, Figure 2S).[28]

TEM images revealed high-order 3-D mesostructure symmetries with a considerable degree of regularity. The images for selected particles of HOM-7 (cubic *Pn*3*m*), HOM-5 (cubic *Ia*3*d*), HOM-3 (3-D hexagonal $P6_3/mmc$), and HOM-1 (cubic *Im*3*m*) (see Supporting Information, Figures 3S, 4S) revealed a uniform 3-D mesopore connecting the structure lattices and running along the respective directions.

In all of the microemulsion systems studied here, the mesophase geometrical shape was not affected by the addition of C_6 and C_7 hydrocarbon, except for the microemulsion lamellar phase (Table 1). However, hexagonally 2-D structural lattice (*P*6*mm*) was successfully synthesized over a range of microemulsion mixture compositions with hexane (C_6) and heptane (C_7) in the lamellar phase (as shown in Figure 11b). Note that the lattice parameters of HOM-*n* materials (i.e., with phase transition) were larger than those of materials synthesized without the phase transition (Table 3), indicating that the swelling of alkanes was significantly effective within the phase transition between the cubic symmetries.[45]

4. Effect of the Solubilizing Agent on Mesopore Structure. The effect of the molar ratio of Brij 56/alkane on the mesophase geometrical shape and its stability was studied by using various molar ratios of Brij56/dodecane in the microemulsion liquid crystal of hexagonal *P*6*mm* phase (50 wt % of Brij 56/TMOS) under ambient synthetic conditions (Table 4). The XRD pattern for a Brij 56:dodecane molar ratio of 2:0.25 (Figure 7a) showed five different peaks, as expected for a long-range ordered hexagonal lattice with d_{100} spacing of 5.2 nm.[2,21] This result indicates that this amount of solubilizing agent was not sufficient to affect the interfacial curvature of the hydrophobic−hydrophilic aggregate. In general, all microemulsion phases with the same additive ratio of Brij 56:dodecane (2:0.25) revealed a swollen aggregate without phase transformation, consistent with the same effect in the hexagonal phase, except the microemulsion lamellar phase. The lamellar bilayered mesostructures of HOM-6 were transformed into the 3-D hexagonally symmetric ($P6_3/mmc$) mesoporous silica structure of HOM-3 (Figure 11c). A slight increase in the amount of cosolvent (dodecane) in the molar ratio composition to 2:0.5 yielded bulk well-defined XRD reflection peaks (Figure 7b), indicating a complete phase change to high-quality 3-D cubic *Pm*3*n* mesoporous silicate, as clearly revealed by the XRD data in Figure 5a. The XRD data revealed the formation of cubic *Pm*3*n* mesoporous silicate with regular 3-D network architecture, even with a Brij 56:dodecane molar

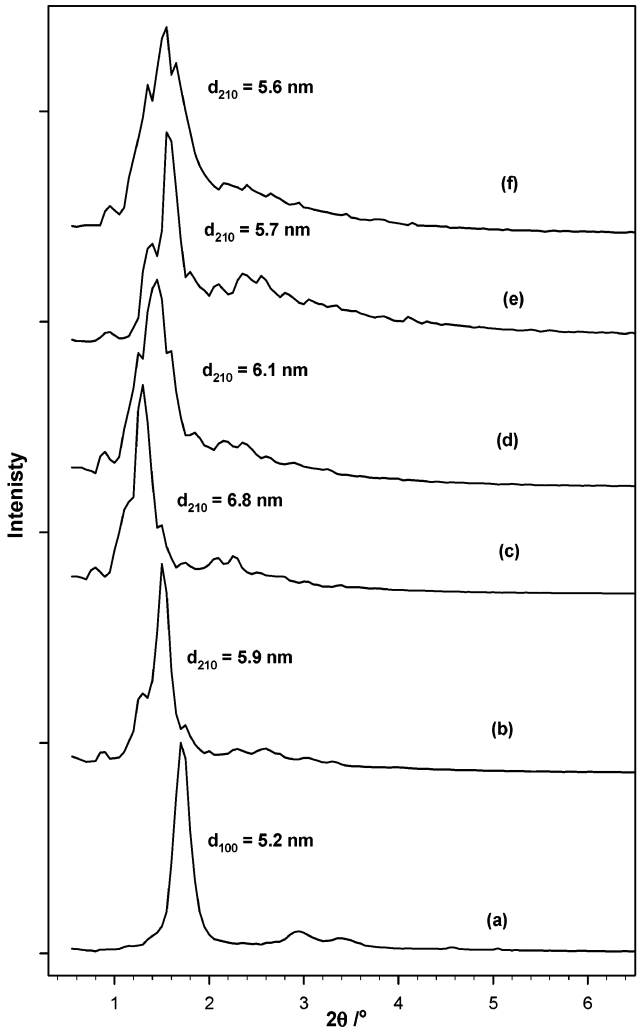

Figure 7. Phase transition study for various molar ratios of Brij 56:dodecane into hexagonal *P*6*mm* microemulsion lyotropic liquid crystal composition of 50 wt % Brij 56/TMOS. XRD patterns of calcined mesoporous silica monoliths using a Brij 56:dodecane molar ratio of (a) 2:0.25, (b) 2:0.5, (c) 2:1, (d) 1:1, (e) 1:2, and (f) 1:3.

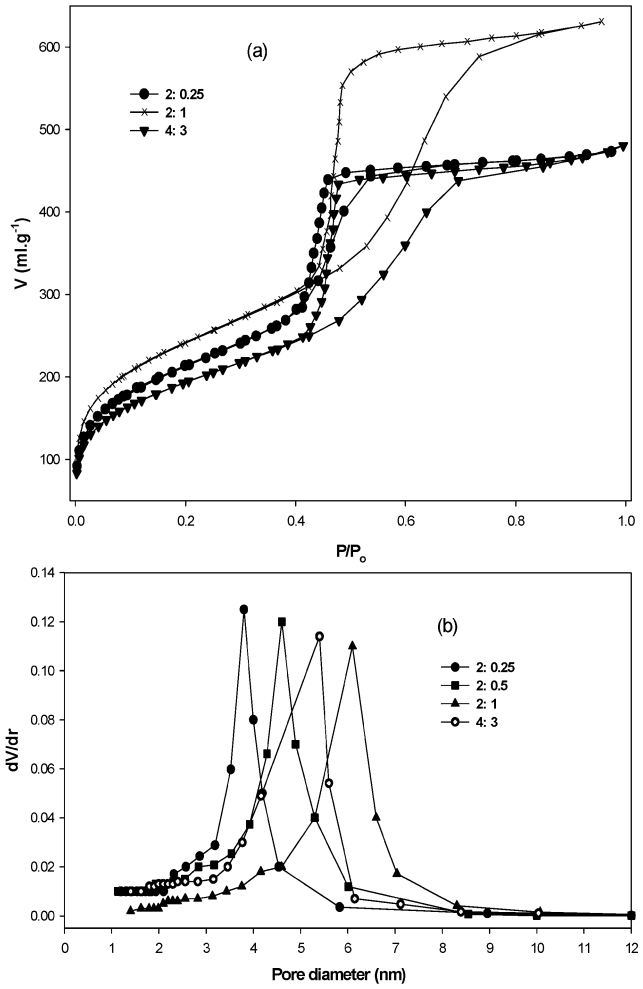

Figure 8. Effect of molar ratio of Brij 56:dodecane incorporated into hexagonal *P*6*mm* (50 wt % of Brij56/TMOS) microemulsion compositions on (a) N_2 adsorption/desorption isotherms and (b) BJH pore size distribution of synthesized mesoporous silica monoliths.

ratio as high as 1:3 in the microemulsion composition. Further addition of cosolvent above a 1:3 molar ratio made the fabrication of monolithic mesoporous silicate difficult under the sol−gel synthetic conditions. The difficulty might be attributed to reduced gelation (solidification) within the microemulsion composition during the interaction between the aggregate and alkane.[44] This effect of reduced gelation on the fabrication led to a high percentage of alkane amount remaining without incorporation into the micellar structure in the microemulsion system, thus governing the loss of the translucent monolithic form.

Clearly evident was that the phase transition from hexagonal (*P*6*mm*) to cubic (*Pm*3*n*) mesophase occurred by using an appropriate amount of alkane in the microemulsion system (Figure 7b). The results here suggest that the interface geometrical shape of the amphiphile could be modified by an appropriate amount of incorporated alkane for phase transition to occur. Any further addition of alkane swelled the aggregates, while the overall cubic structures were maintained with different unit cell dimensions (Table 4 and Figure 7b−f). Highly ordered cubic *Pm*3*n* with the largest a_o was observed at a Brij 56:alkane molar ratio of 2:1 (Table 4, Figure 5a). The crystalline 3-D structure did not dramatically change by increasing the amount of alkane in the microemulsion compositions, as evidenced by the retention of the highly ordered XRD patterns (Figure 7e,f).

Furthermore, N_2 adsorption/desorption isotherms confirmed the effect of increasing the amount of solubilizing agent in the microemulsion composition upon the mesoporous pore architectures (Figure 8). The pore size expanded upon increasing the amount of solubilizing agent in the phase aggregates (Table 4). Also, the hysteresis loops increased with increasing mesopore size (Figure 8a). The pore size significantly increased when the Brij 56:alkane molar ratio increased to about 2:1 in the microemulsion liquid crystal phases, in agreement with the XRD data (Figure 7). This means that, to produce large mesopores and stable mesoporous silica structures, the optimal molar ratio of Brij 56: alkane in the microemulsion system was 2:1. The slight decrease in mesopore size with increasing molar ratio might be due to the partial solubilizing effect with the micelle (Figure 8b). The sharp peaks in the pore size distribution found for all molar ratios were due to the

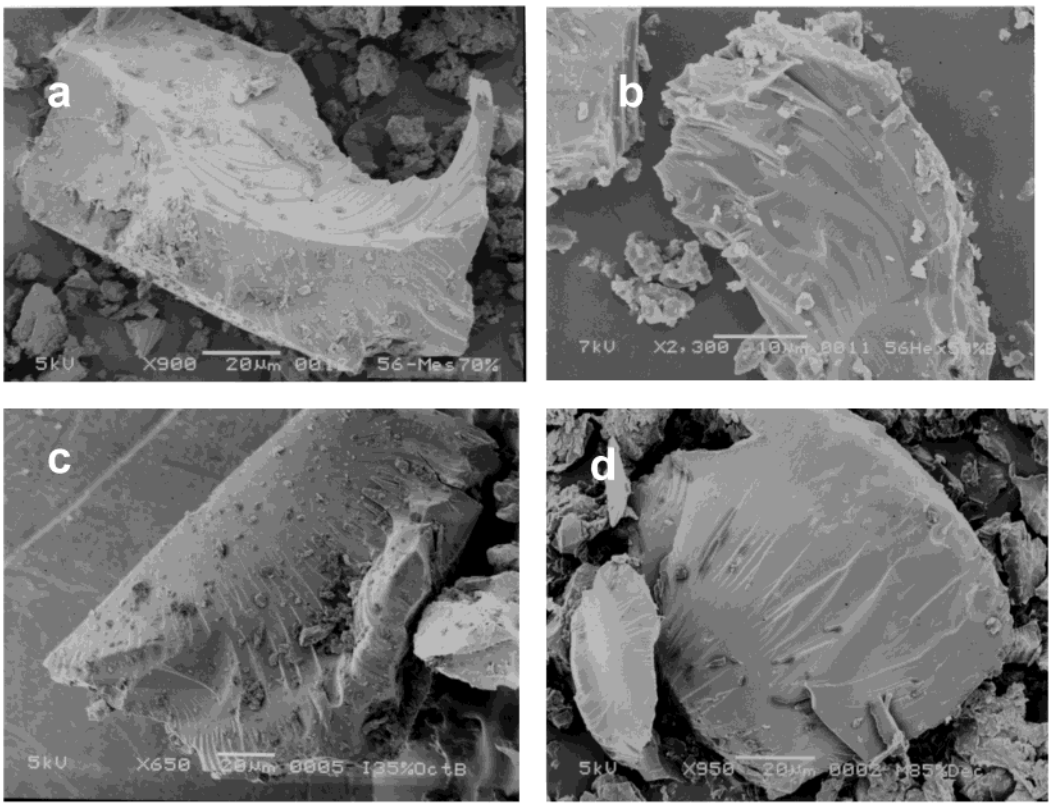

Figure 9. Representative SEM images of particle morphologies. (a) Cubic *Ia*3*d* (HOM-5) synthesized by incorporating octane into microemulsion liquid crystal of the cubic *Ia*3*d* phase of Brij 56/TMOS (70 wt %). (b) 3-D hexagonal $P6_3/mmc$ (HOM-3) synthesized by incorporating octane into microemulsion liquid crystal of the hexagonal phase of Brij 56/TMOS (50 wt %). (c) Cubic *Pm*3*n* (HOM-9) synthesized by incorporating nonane in microemulsion systems with the cubic *Im*3*m* liquid crystal phase of Brij 56/TMOS (35 wt %). (d) Cubic *Pn*3*m* (HOM-7) synthesized by incorporating decane into microemulsion liquid crystal cubic *Pn*3*m* phase (85 wt %).

high degree of uniformity in the mesopore architectures.[47]

5. HOM-*n* Particle-Texture Morphology. SEM images of the HOM-n silica samples (Figure 9) revealed various crystal-like morphologies of the surface particles. The cubic *Ia*3*d* (HOM-5) and 3-D hexagonal *P*63/*mmc* (HOM-3) mesoporous particles exhibited boat- and rose-shaped morphology, respectively. The specific morphologies of the particles were characteristically plate-like with fine lines upon the surface (as shown in Figure 9c,d). In addition, the face-centered cubic *Fm*3*m* and the cubic *Im*3*m* samples exhibited well-defined disk-shaped and large-diameter spherical particle morphologies (see Supporting Information, Figure 5S). In general, all the phase domains had large particles (20 μm in diameter) with smooth surfaces, reflecting the high mesoscopic crystalline level.[28,48] These results indicate that microemulsion mesophases can be applied to form well-known morphological mesporous silica structure with distinct particle shape and size.

6. Control of Mesopore Organization by Using Microemulsion Systems. Our results show that the templating of microemulsion lyotropic liquid crystal phases allows a high level of control and adjustability over the mesopore size and structure morphology of the 3-D mesoporous materials. N_2 adsorption/desorption isotherms are reliable to investigate the periodicity of cubic mesoporous architectures. The isotherms of all the mesoporous samples synthesized here displayed type IV characteristics (Figure 10A), typical of mesoporous materials. The pore condensation of large-pore materials that are synthesized via the phase transition between the cubic symmetries in the microemulsion systems exhibited large hysteresis loops. These large hysteresis loops seemed to be intermediate between H_2- and H_1-types, indicating a high degree of pore connectivity with large channel-like pores.[10,27] The width of the hysteresis loop increased with increasing mesopore size. The well-known sharp inflection point appeared at $0.4 \leq P/P_o \leq 0.8$ depending on the pore size, indicating capillary condensation within uniform mesopores. As the alkyl chain length of alkane used for the formation of the microemulsion system was increased, the position of the capillary condensation step gradually shifted to higher relative pressure (Figure 10Aa−d). This shift revealed a systematic increase in pore size, which was expected from the incorporation of the long alkyl chain lengths of hydrocarbons into the core of the micellar aggregate in each lyotropic phase.

Barrett−Joyner−Halenda (BJH) analyses revealed narrow peaks for all mesoporous samples, indicating well-defined uniform pores in the materials (Figure 10B).[49] The pore size depended on the accessible range of hydrophobic (C_{16} hydrocarbon chain) and hydrophilic (EO_{10}) block lengths of Brij 56. Therefore, the pore size

(47) El-Safty, S. A.; Evans, J.; El-Sheikh, M. Y.; Zaki, A. B. *Colloids Surf. A* **2002**, *203*, 217.

(48) Blin, J. L.; Léonard, A.; Su, B. L. *Chem. Mater.* **2001**, *13*, 3542.

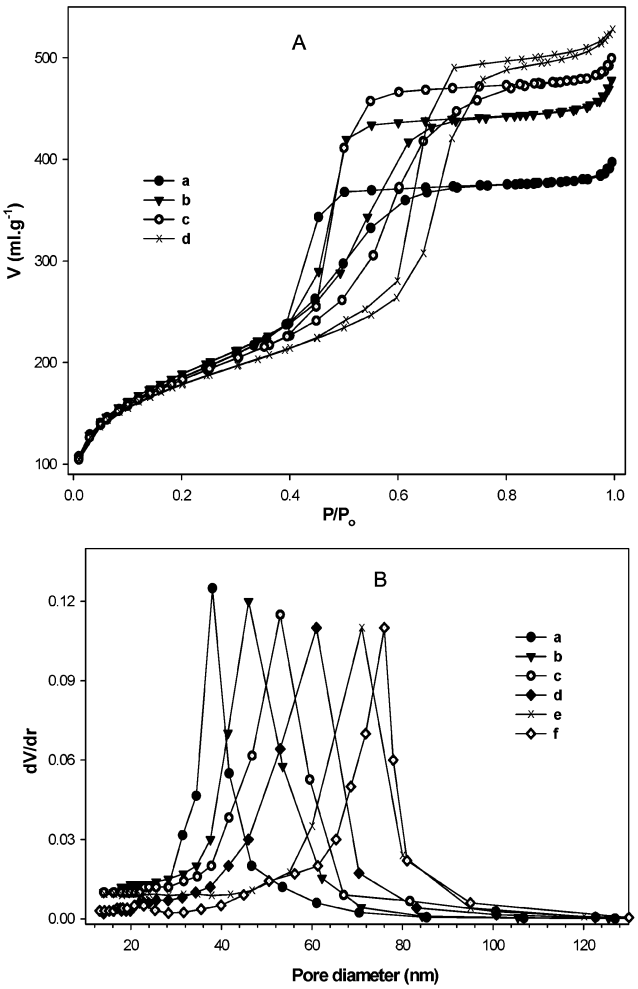

Figure 10. N_2 adsorption/desorption isotherms at 77 K (A) of calcined cubic *Pm*3*n* mesoporous silica monoliths (HOM-9) synthesized by incorporating (a) octane into the cubic *Im*3*m* liquid crystal phase of 35 wt % Brij 56/TMOS, (b) nonane and (c) decane into the hexagonal liquid crystal phase of 50 wt % Brij 56/TMOS, and (d) dodecane into the cubic *Pn*3*m* liquid crystal phase of 85 wt % Brij 56/TMOS in microemulsion systems. Pore size distribution of HOM-9 monoliths using BJH model from the adsorption branch isotherm (B) synthesized by incorporating cosolvents of (a) octane into the cubic *Im*3*m* phase of 35 wt % Brij 56/TMOS, (b) nonane, (c) decane, and (d) dodecane into the hexagonal phase of 50 wt % Brij 56/TMOS, and (e) dodecane and (f) pentadecane into the cubic *Pn*3*m* phase of 85 wt % Brij 56/TMOS in microemulsion sol−gel compositions.

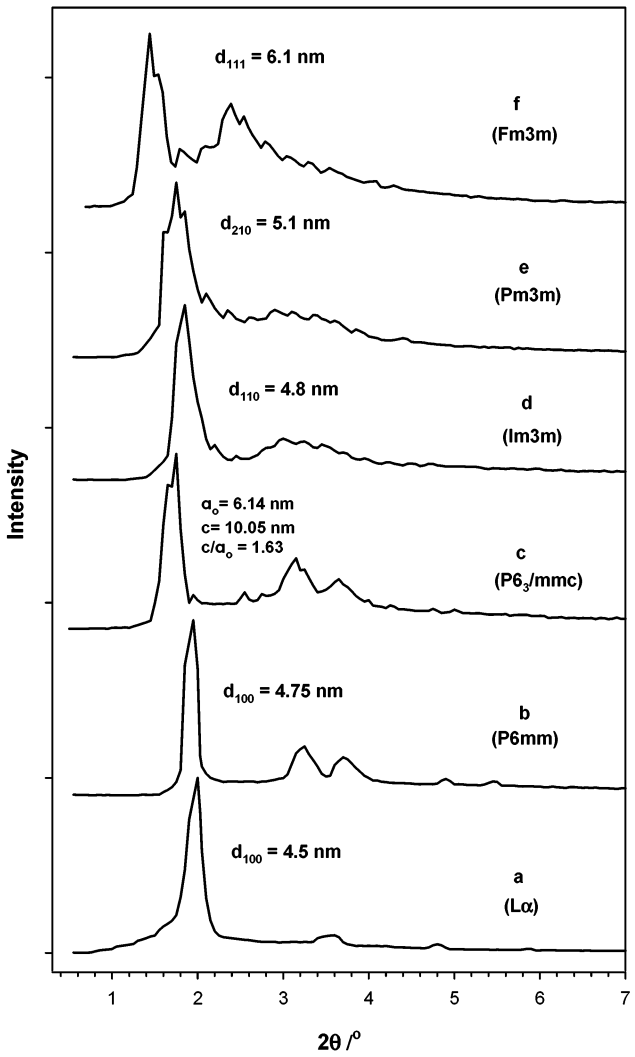

Figure 11. Effect of the alkyl chain length of the cosolvent incorporated into the lamellar liquid crystal phase of Brij 56/TMOS 75 wt % on the geometrical phase transition. XRD patterns of mesoporous silica materials of (a) lamellar structure (HOM-6) synthesized in the absence of the microemulsion system. (b) 2-D hexagonal *P*6*mm* (HOM-2) synthesized by incorporating heptane, (c) 3-D hexagonal $P6_3/mmc$ (HOM-3) synthesized by incorporating dodecane at a molar ratio of 0.25: 2 with Brij 56, (d) cubic *Im*3*m* (HOM-1), (e) cubic *Pm*3*m* (HOM-4), and (f) cubic *Fm*3*m* (HOM-10) synthesized by incorporating octane, nonane, heptadecane, respectively, into lamellar (L_∞) phase.

of the mesoporous samples significantly increased with the incorporation of alkane into the micelle. This significant increase was accompanied by a phase transition between the cubic symmetries, indicating that the interpenetration of alkane into hydrophobic or hydrophobic−hydrophilic regions of the micelle mainly affected the hydrophobic volume and the effective cross-sectional area of the hydrophilic group during the phase geometrical transition (Scheme 4).[45,50] In our microemulsion systems, the swelling simultaneously occurred with the interpenetration of alkanes during the re-self-organization of aggregates during the formation of the microemulsion systems. Control of the large pore size was achieved by the addition of C_{12} alkyl chain (dodecane) in the microemulsion composition systems, due to the significant solubilization with the micelle.[20] The increase in the alkane length (C_{15}–C_{19}) in the microemulsion systems led to a slight decrease in the mesopore size of HOM-*n* materials, indicating the partial solublization of the alkane into the micelle. This partial solublization behavior indicates that some of the alkane component, especially the high molecular weight alkanes, might not be involved in the actual templating of the mesopore structures. Although only partial solubilization occurred when alkanes with long alkyl chains (C_{15}−C_{19}) were incorporated into a micelle and thus decreased the pore size, the level of solubilization was sufficient to induce change in the phase geometrical shape (Tables 1−3).

(49) Barrett, E. P.; Joyner, L. G.; Halenda, P. P. *J. Am. Chem. Soc.* **1951**, *73*, 373.

(50) Feng, P.; Bu, X.; Pine, D. J. *Langmuir* **2000**, *16*, 5304.

Therefore, the HOM-*n* mesoporous silicate monoliths had a high total pore volume (0.8−1.5 cm^3/g) and BET surface area, suggesting highly ordered pore architecture. The pore wall thickness was estimated by subtracting the BJH pore size from the unit cell parameter (a_o) of the lattice structures. The large wall thickness was related to the large unit cell dimension. The thickness of the pore wall structure is governed by the organic−inorganic composites of the mutually interpenetrating network of silica and $C_{16}EO_{10}$ species. The estimated thickness of the silicate wall was large due to the use of microemulsion systems in the direct templating methodology. However, the addition of the alkane into the interior micelle aggregate enhanced the extent of the polymerization of the silicon alkoxide around the phase assembly, leading to a thicker silicate wall than that reported previously with M41S and SBA materials and with HOM materials synthesized via a lyotropic phase template.[2,10,28] The wall was thick when the sample had a large surface area (Tables 2 and 3), consistent with MCM-like materials synthesized by using CTAB of $C_{12-}C_{18}$ hydrocarbon chain length.[51] Our results here indicate that the microemulsion liquid crystal templating methodology can significantly improve the mesopore domains; such domains will thus have large, regular architecture with thick walls.

7. Mechanistic Feature of the Phase Transition between HOM Types. Direct templating by using microemulsion liquid crystal mesophases is a methodology that allows an additional level of control over the surfactant mesophase domains and the mesopore organizations, compared with other synthetic methods.[10,22,27] We previously reported that seven mesophase structures with restrictive pore sizes up to 35 Å can be synthesized by using the lyotropic liquid crystal phase as a template at different high concentration ratios of Brij 56 surfactant.[28] In our current study, by applying this method to the lamellar phase of Brij 56 (75 wt %), for example, the primary phase could be controlled throughout the formation of various types of phases with highly ordered structures (Figure 11b−f), indicating the sensitivity of the change in geometrical shape of phases within the microemulsion compositions to the solublization of alkane into the surfactant phase aggregates. Figure 11 also shows that the lamellar structures that had high micelle packing were unstable forms, even with addition of short alkyl chain length (C_6, C_7 hydrocarbon) in the microemulsion lamellar system. However, the XRD pattern (Figure 11a) revealed that the well-defined lamellar order with *d* spacing ratios of $1:{}^1/_2:{}^1/_3:{}^1/_4$ was only obtained by using lyotropic liquid crystalline phase at Brij:TMOS (75 wt %) ratio,[28] indicating that the high curvature of the surface interface of the phase assemblies were preferably generated in these microemulsion systems. In addition, XRD patterns (Figure 11) revealed that the highly ordered diffraction peaks were evident in all mesoporous silica structures, suggesting that the crystalline structures were maintained with the enlargement in the pore dimension of the lattices. In general, the geometrical phase transition structures in the microemulsion (Brij 56/alkanes/H_2O/TMOS) systems can be described as in Scheme 3.

This systematic sequence (Figure 11, Table 1) helps clarify how the phase transition can occur in the presence of the solubilizing agent (alkane) with the surfactant aggregates. In the synthesis microemulsion systems, our results show that (i) no structural change in the primary crystalline phases occurred upon addition of the alkanes with short alkyl chain length (C_6, C_7 hydrocarbon), except with addition to the lamellar phase (Figure 11); (ii) the phase transition and effective swelling occurs upon addition of long alkyl chain of alkanes (C_9-C_{19} hydrocarbon) to the primary crystalline phases; (iii) several kinds of cubic phases, such as $Fm3m$, $Pm3m$, and $Pm3n$, were only fabricated as a result of the phase transition in the microemulsion systems; and (iv) the mesophase structural change was not only influenced by the alkane type but also by the additive amount of alkane to the mesophase aggregates (Table 4). In general, the transitions between the mesophase structures were primarily driven by the surfactant interfacial curvature in the micelle. The micelle shape geometry is based on the surfactant packing parameter, which describes the surface interfacial curvature of the micelle.[14,52,53] The critical packing parameter (Q) can be represented as $Q = v/a_s l_c$, where v is the volume occupied by the hydrophobic portion of the amphiphile, a_s is the effective cross-sectional area of the amphiphilic headgroup surfactant, and l_c is the critical length of the surfactant tail. Specific values of Q are associated with inverted micelles ($Q > 1$), lamellar phases ($Q = 1$), vesicles (${}^1/_2 < Q < 1$), cylindrical micelles (${}^1/_3 < Q < {}^1/_2$), and spherical micelles ($Q < {}^1/_3$).[52,53] Low Q values yield large interfacial surface curvatures.[53] Our current study shows that cubic mesophase geometries with large surface curvatures that are domains can be fabricated in microemulsion systems with addition of alkanes that have long hydrocarbon chains. Due to the abrupt change in the geometrical shape at the phase transition,[54] it is difficult to determine the net value of Q, particularly with phase symmetries that are almost cubic. On the other hand, the placement and organization of the solublizing agents (alkane) in the micelle during the interaction are mainly responsible for determining the curvature of the surfactant layer interface.[41,55] However, the solublized alkane can feasibly penetrate into different situations of the surfactant layers (Scheme 4).

The spontaneous interfacial curvature is mainly affected by the interaction between alkanes with different alkyl chain length and Brij 56 that might occur in the hydrophobic part, in the hydrophobic−hydrophilic interface, in the aqueous hydrophilic part, and in the core of the surfactant aggregates. These interactions had a crucial influence on the structural changes of the surfactant−silica mesophases in these synthesized microemulsion systems. There is yet no reported evidence to verify whether the interaction is predominant in these microemulsion phases of Brij 56. The long alkyl chain hydrocarbon might solubilize in the deep core of

(51) Kruk, M.; Jaroniec, M.; Kim, J. M.; Ryoo, R. *Langmuir* **1999**, *15*, 5279.

(52) Israelachvili, J. N.; Mitchell, D. J.; Ninham, B. W. *J. Chem. Soc., Faraday Trans. 2* **1976**, *72*, 1525.

(53) Nossal, R.; Lecar, H. *Molecular and Cell Biophysics*; Addison-Wesley: Boston, MD, 1991.

(54) Gruner, S. M. *J. Phys. Chem. B* **1989**, *93*, 7562.

(55) Kunieda, H.; Horri, M.; Koyama, M.; Sakamoto K. *J. Colloid Interface. Sci.* **2001**, *236*, 78.

hydrophobic chains, thus directing the formation of the oil pool inside the surfactant mesophase aggregates.[55] Therefore, the volume of the micelle increased while the effective cross-sectional area per surfactant was kept constant, and hence, the surfactant layer curvature increased. This penetration of alkanes indicates that, in all microemulsion phases, the swelling tendency was accompanied by the phase transition upon addition of long alky chain hydrocarbon. This hypothesis for phase transition in these microemulsion systems coincides with previously reported results for hexagonal H_I–cubic $Pm3n$ and hexagonal $H_I-Im3m-Pm3n$ transitions in the ionic and nonionic surfactants/oil/water systems.[37,45,55] The solublization of the appropriate amount of alkane (C_9-C_{19} hydrocarbon) with the surfactant layers produced changes in the interfacial curvature, thus inducing the phase transition and swelling (Figure 7, Table 4). On the other hand, addition of alkanes with short alkyl chain length (C_6, C_7 hydrocarbon) ineffectively changed or swelled the surfactant interface layers, indicating that the alkanes were dispersed between the hydrophobic (tail) layer without significantly influencing the volume of micelle rather than the alkanes being solublized into the surfactant palisade layer.[56] This solublization of the alkanes might have occurred with lamellar phase to induce the hexagonal structure to change the surfactant interface curvature to a lesser degree with an insignificant increase in the pore dimension (Table 3).

In these microemulsion systems, the 3-D cubic-face, primitive-centered structures might have the largest surface interfacial curvatures among the cubic symmetries synthesized here, and thus the cubic $Fm3m$ and $Pm3n$ geometries are stable phase domains with additive long alkyl chain length ($C_{10}-C_{19}$ range) of alkanes in the microemulsion mesophase systems (Table 1). Accordingly, the surface curvature of the phase assembly in the microemulsion compositions increased in the following order for the mesophases: lamellar (L_∞) < cubic $Ia3d$ < hexagonal ($P6mm$) < 3-D hexagonal ($P6_3/mmc$) < spherical cubic ($Im3m$) < cubic $Pm3m \leq$ cubic $Pn3m \leq$ cubic $Pm3n$ < face-centered cubic ($Fm3m$) (Scheme 3). Tiddy et al. similarly investigated cubic $Fm3m$, $Pm3n$, and $Im3m$ phases formed in the nonionic surfactant of the $C_{12}EO_{12}$/water binary system. They reported that the maximum volume fraction related to the critical packing factor increases in the following order: body-centered cubic ($Im3m$) < face-centered cubic ($Fm3m$) < cubic $Pm3n$ < hexagonal H_I < lamellar (L_∞).[57] The phase transitions of the $C_{12}EO_{12}$/water binary system were similar, to a great extent, to that found in microemulsion systems of $C_{16}EO_{10}$/alkanes/H_2O that we studied here (Scheme 3).

During the phase transition, the preferable cubic phase geometry was identifiably formed depending on the effective solublization of alkanes into the micellar phase assembly at a definite temperature and composition (Table 1). In this solublization, the interior micelle acquired a degree of conformational freedom as a result of constraint by the incorporated alkyl chain.[44] This degree of freedom allowed the rearrangement and deformation of the micelle in accordance with the appropriate surface curvature of the shape of the formed geometrical phase.[57] This significant feature, namely, the degree of conformational freedom, explains (i) the extent of control that each primary phase assembly (formed at definite Brij 56:TMOS mass ratio) had over the structural changes during the phase transition, particularly with addition of $C_{8-}C_{12}$ alkyl chain lengths (as shown in Table 1), and (ii) why not just one but both the cubic $Fm3m$ and $Pm3n$ phase structures were predominant and stable in the microemulsion systems of Brij 56 template.

Our results suggest that the synthetic methodology that uses microemulsion liquid crystal template can generate nanostructured materials with large uniform monoliths, can effectively control the mesopore morphological structures, can fabricate millimeter-sized particles that have a high degree of crystallinity, and can fabricate various geometrical cubic mesophases of materials.[58] This simple, fast method can fabricate silica monoliths without loss of significant long-range ordered structure.[34,59] A potential advantage of mesoporous silica (HOM-*n*) produced via this methodology is thicker and denser walls than materials synthesized with other routes, and thus will improve the thermal and mechanical stability of the mesoporous silica materials.

8. Conclusion. Structure-directed assembly by using a microemulsion liquid crystal template extended the degree of control over the amphiphilic mesophase domains and the pore size morphology. Furthermore, the fabrication of large monoliths with highly crystalline particles was realistically achieved. In this methodology, the addition of alkanes with various lengths of hydrocarbon chains in adjustable microemulsion phases allowed synthesis of highly ordered, large-caged cubic mesoporous silica HOM-*n* monoliths, including spherical cubic $Im3m$ (HOM-1), 3-D hexagonal $P6_3/mmc$ (HOM-3), cubic $Ia3d$ (HOM-5), cubic $Pn3m$ (HOM-7), cubic $Pm3n$ (HOM-9), cubic $Fm3m$ (HOM-10), and cubic $Pm3m$ (HOM-4) structures. The solubilization process of alkanes within the micelle at each lyotropic mesophase determined the preferable cubic mesophase structures. XRD and TEM analyses revealed that the formation of highly ordered cubic mesoporous structures was arranged over uniform arrays of all cubic lattices. N_2 isotherms revealed that swelling of the aggregates accompanied the phase transition process and that the pore size significantly increased with the mesophase transition between different cubic symmetries. The phase transition occurred with the addition of long alkyl chains in microemulsion lyotropic mesophases, particularly chains longer than C_7 (heptane). The transitions between the mesophase structures were primarily governed by the surfactant interfacial curvature in the micelle This simple, fast method will enable the fabrication of other high-grade mesoscopic organizations by using templates that have high molecular mass. Our results demonstrate that this direct templating methodology can successfully fabricate a variety of

(56) Jonsson, B.; Lindman, B.; Holmberg, K.; Kronberg, B. *Surfactants and Polymers in Aqueous Solution;* Wiley: Chichester, 1998.
(57) Sakya, P.; Seddon, J. M.; Templer, R. H.; Mirkin, R. J.; Tiddy, G. J. T. *Langmuir* **1997**, *13*, 3706.
(58) Feng, P.; Bu, X.; Stucky, G. D.; Pine, D. J. *J. Am. Chem. Soc.* **2000**, *122*, 994.
(59) Evans, J.; Zaki, A. B.; El-Sheikh, M. Y.; El-Safty, S. A. *J. Phys. Chem. B* **2000**, *104*, 10271.

nanoporous composites in a large range of pore size (about 30−80 Å), high surface area (900 m^2/g), and thicker wall architectures, while the long-range ordered uniform structure for various 3-D networks is maintained.

Acknowledgment. We are grateful to Prof. S. Niwa and Dr. K. Sato, from the AIST Institute, Tohoku Centre, Sendai, Japan, for critical assistance, and to the Japan Society for the Promotion of Science (JSPS) for financial support.

Supporting Information Available: XRD patterns and TEM micrgraphs of 3-D mesoporous silica monoliths and representative SEM images of particle morphologies (PDF format). This material is available free of charge via the Internet at http://pubs.acs.org.

CM034282O